Quaternary Science Reviews 124 (2015) 145–161

Contents lists available at ScienceDirect

Quaternary Science Reviews

journal homepage: www.elsevier.com/locate/quascirev

Panigarh cave stalagmite evidence of climate change in the Indian Central Himalaya since AD 1256: Monsoon breaks and winter southern jet depressions

Fuyuan Liang [a, *], George A. Brook [b], Bahadur S. Kotlia [c], L. Bruce Railsback [d], Benjamin Hardt [e], Hai Cheng [e, f], R. Lawrence Edwards [e], Selvaraj Kandasamy [g]

[a] Department of Geography, Western Illinois University, Macomb, IL 61455, USA
[b] Department of Geography, University of Georgia, Athens, GA 30602, USA
[c] Centre of Advanced Study in Geology, Kumaun University, Nainital 263002, India
[d] Department of Geology, University of Georgia, Athens, GA 30602, USA
[e] Department of Geology and Geophysics, University of Minnesota, Minneapolis 55455, USA
[f] College of Global Environmental Change, Xi'an Jiaotong University, Xi'an, Shaanxi 710049, China
[g] State Key Laboratory of Marine Environmental Science, Xiamen University, Xiamen 361102, China

ARTICLE INFO

Article history:
Received 23 February 2015
Received in revised form
27 June 2015
Accepted 14 July 2015
Available online 26 July 2015

Keywords:
Medieval Climate Anomaly
Little Ice Age
Stalagmite
Isotopes
Petrography
Himalayas
Indian Summer Monsoon
Monsoon breaks

ABSTRACT

Variations in petrography, stable isotopes, reflectance, and luminescence along the central growth axis of a 14.5 cm stalagmite from Panigarh cave indicate cooler and slightly wetter conditions in the Himalayan foothills of northern India during the Little Ice Age (LIA), which lasted from ~AD 1489–1889 based on deposition of calcite, and AD 1450–1820 based on rapid changes in $\delta^{18}O$ values. Conditions were warmer and drier during the preceding Medieval Climate Anomaly (MCA) and also in the post-LIA periods, as evidenced by deposition of aragonite. A review of currently existing stalagmite and other proxy data from south and east Asia reveals a broad spatial pattern in precipitation over south and east Asia during the LIA, with northern areas showing generally increased precipitation and southern areas reduced precipitation. During the MCA and after the LIA, the records suggest this pattern was reversed. Weaker ISM during the LIA brought drought conditions to the core ISM area but triggered more monsoon 'breaks' that brought higher precipitation to the Himalayas. At the same time, the weaker ISM may also have pushed more depressions along the path of the southern winter jet which brought more winter precipitation to the Himalayas and therefore a LIA wetter in our study area.

Published by Elsevier Ltd.

1. Introduction

The Indian Summer Monsoon (ISM) is crucial to the people of India and elsewhere in South Asia. Two-thirds of Indians depend on farm income and over 40% of the cropped area has no form of irrigation other than the rains. More than half of India's farm output comes from summer crops dependent on the ISM. For good crop production, the rains have to be not just robust but also evenly spread across states. The ISM also replenishes 81 nationally-monitored water reservoirs vital for drinking, power and irrigation (Haq and Choudhury, 2014). The health of the Asian Summer Monsoon (ASM) affects 60% of the Earth's population as it provides the water needed for agriculture and industry (Davis et al., 2005). It is therefore, important to understand how the ASM varies over time and the factors that are responsible for changes in its strength.

Although fickle today, the ISM may have been much weaker in the past for long periods of time, particularly during the Little Ice Age (LIA) and other cold intervals of the Holocene (Anderson et al., 2002, 2010; Gupta et al., 2003). A weaker monsoon should bring less precipitation across the Asian mainland. However, the data are ambiguous with much recent evidence suggesting wetter conditions during at least certain episodes of the LIA in Nepal (Denniston et al., 2000), northern India (Rühland et al., 2006; Kotlia et al., 2012, 2014; Duan et al., 2013; Sanwal et al., 2013), and southern China (Chu et al., 2002; Chen et al., 2005) as well as northwestern China (Chen et al., 2009). However, no high-magnitude flood deposits have been identified in the six large rivers crossing central and western India suggesting that there was no really intense

* Corresponding author.
E-mail address: F-Liang@wiu.edu (F. Liang).

http://dx.doi.org/10.1016/j.quascirev.2015.07.017
0277-3791/Published by Elsevier Ltd.

precipitation at this time and in fact that the conditions were probably drier from the 14th to the 19th centuries (Kale and Baker, 2006). Looking at the ambiguous and uncertain data set, it is obvious that more information is needed to elucidate conditions during the LIA. This paper presents evidence from a stalagmite (PGH-1) from Panigarh cave near Pithoragarh in northern India, located in the southern foothills of the Himalayas. The stalagmite was active when collected in 2006 and preserves evidence of variations in the ISM during the past ~750 years, including the period of the LIA. Multi-proxy data from the stalagmite, including variations in stable isotopes, reflectance, U–V stimulated luminescence, and petrography, provide data on climate during the Medieval Climate Anomaly (MCA) and LIA in this area. Neither of these periods appears to have been synchronous across the globe. The MCA lasted from about AD 950 to 1250 (Mann et al., 2005) and the LIA from AD 1550–1850 with three cold intervals at ~AD 1650, 1770, and 1850 (NASA) or alternatively, from about AD 1350 to about 1850 (IPCC Fourth Assessment Report: Climate Change, 2007).

The climate of India is dominated by the ISM but has distinct warm and cold seasons. During winter the upper westerlies over Asia split into two currents, one north and the other south of the high Tibetan (Qinghai–Xizang) Plateau and re-join off the east coast of China. The two jet stream branches have been attributed to the disruptive effect of the topographic barrier to airflow. However, the stronger southern branch over northern India corresponds to a strong latitudinal thermal gradient (from November to April). Air subsiding beneath the upper westerly current gives dry outblowing northerly winds from the subtropical anticyclone over NW India and Pakistan. Surface winds are NW over most of northern India. Important is the steering of winter depressions over northern India by the upper jet. The lows, which are not usually frontal, appear to penetrate across the Middle East from the Mediterranean and are important sources of rainfall for northern India and Pakistan, especially as it falls when evaporation is at a minimum. It is significant that the mean axis of the winter jet stream over China shows a close correlation with the distribution of winter rainfall. In the rear of these depressions are invasions of very cold air. In fact, winter mean temperatures in less-protected southern China are much lower than in India (Barry and Chorley, 2003).

In early summer, generally during the last week in May, the southern branch of the high-level jet begins to break down, gradually shifting northward over the Tibetan Plateau. There is a variable pulse alternating between active and break periods during the May to September summer monsoon flow. During active periods the convective monsoon trough is located further north giving heavy rain over north and central India and the west coast. During break conditions, the Intertropical Convergence Zone (ITCZ) shifts to the south, the easterly jet weakens and subsiding air is forced to rise by the Himalayas along a break trough located above the foothills, which replaces the monsoon trough during break periods (e.g. Ramaswamy, 1962). This circulation brings rain to the Himalayan foothills and Brahmaputra valley at a time of generally low rainfall elsewhere. The shift of the ITCZ to the south is accompanied by a similar southward movement and strengthening of the westerly jet to the north weakening the Tibetan anticyclone. The lack of rain over much of the subcontinent during break periods may be due in part to the eastward extension across India of the subtropical high-pressure cell centered over Arabia at this time. During October the westerly jet re-establishes itself south of the Tibetan Plateau and cool season conditions are restored (Barry and Chorley, 2003).

2. Panigarh cave

Panigarh cave (29°33′10″ N; 80°07′03″ E; 1520 m amsl) is 300 km northeast of New Delhi, 30 km west of the western boundary of Nepal, and 1.5 km west of Boonga Village (Fig. 1). On January 6, 2006, an active, 14.5 cm long stalagmite (PGH-1) was collected from a 4 m long cave with an entrance of 1.4 m^2. The cave is developed in the Precambrian Thalkedar Limestone extending about 250 m above the cave with a surface cover of about 80 cm thick brown–black soil. The vegetation is largely C_3 being composed predominantly of *Pinusroxburghii* with small shrubs, grasses and herbs. The climate is subtropical monsoon with wet, warm summers and drier, cooler winters. Annual precipitation is 1260 mm, about 80% falling during the monsoon season from June to September. At Pithoragarh, 9 km NW of Panigarh cave, the mean annual temperature is 17.4 °C ranging from 7.7 °C in January to 23.6 °C in June (Kotlia et al., 2000, see Table 1).

3. Materials and methods

The PGH-1 stalagmite was cut along the central growth axis. After polishing, one of the exposed surfaces was scanned at 300 dpi spatial resolution and 8 bit (256 increments) gray level resolution. It was then illuminated by long-wave ultraviolet light (320–420 nm wavelength) from two Macken Instruments Model 22-UV lamps in a darkroom. Luminescence from the stalagmite was recorded by a Nikon D-70, 6-megapixel digital camera fitted with a Kodak Wratten Gelatin Filter #2E to prevent transmission of the UV excitation energy band. Variations in reflectance and luminescence were measured along a 10-pixel-wide traverse down the central growth axis of the stalagmite using image analysis software. Gray-level (0 = black; 255 = white) and luminescence (0 = black; 255 = white) values have a spatial resolution of 0.07 mm (i.e., ~0.6 year per dot).

Thin sections for petrographic study were prepared from the other half of the stalagmite. Five samples of ~100 mg were drilled at 6, 25, 70, 110, and 140 mm from the top of the stalagmite for ICP-MS U-series dating following procedures outlined in Edwards et al. (1987), Cheng et al. (2000), and Shen et al. (2002). Ages were calculated using half-lives listed in Cheng et al. (2000) and are reported with 2σ analytical errors.

Powdered material for stable isotope analysis was removed by drilling at intervals along the central growth axis of PGH-1. In the upper and lower aragonite sections of the stalagmite, samples of 50–100 μg were drilled at 1.5–2 mm intervals. Fourteen samples were processed at the Savannah River Ecology Laboratory, University of Georgia, on a Finnigan Deltaplus XL isotope ratio mass spectrometer operated in continuous flow mode (CF-IRMS) using a Gasbench II peripheral device (Jimenez-Lopez and Romanek, 2004), with analytical precision (1σ) ±0.14‰ for $\delta^{13}C$ and ±0.23‰ for $\delta^{18}O$, based on the repeated measurements of the NBS-19 standard. Another 27 samples were processed in the Department of Geology Stable Isotope Laboratory at the University of Alabama in Tuscaloosa on a Finnegan Deltaplus or Delta V isotope ratio mass spectrometer using a GasBench-IRMS system following methods discussed in Lambert and Aharon (2011). Reproducibility for both $\delta^{13}C$ and $\delta^{18}O$ was ±0.1‰ based on NBS-19 and sample repeats.

In the central section of PGH-1, which consists of variable portions of calcite and aragonite, 30samples of 10–20 mg were drilled at 2.5 mm intervals. These samples were first subjected to XRD analysis to establish percentage aragonite and percentage calcite; then $\delta^{13}C$ and $\delta^{18}O$ were determined on the very same samples in the University of Georgia, Department of Geology Stable Isotope Laboratory on a Finnegan Delta E ratio Mass Spectrometer with precision of 0.04‰ for $\delta^{13}C$ and 0.05‰ for $\delta^{18}O$ based on repeated measurements with the NBS-19 standard.

Aragonite is enriched in ^{13}C by 1.7‰ (Romanek et al., 1992) and in ^{18}O by 1.0‰ (Grossman and Ku, 1986) compared to calcite when deposited from water with the same $\delta^{18}O$ and $\delta^{13}C$ values. As the

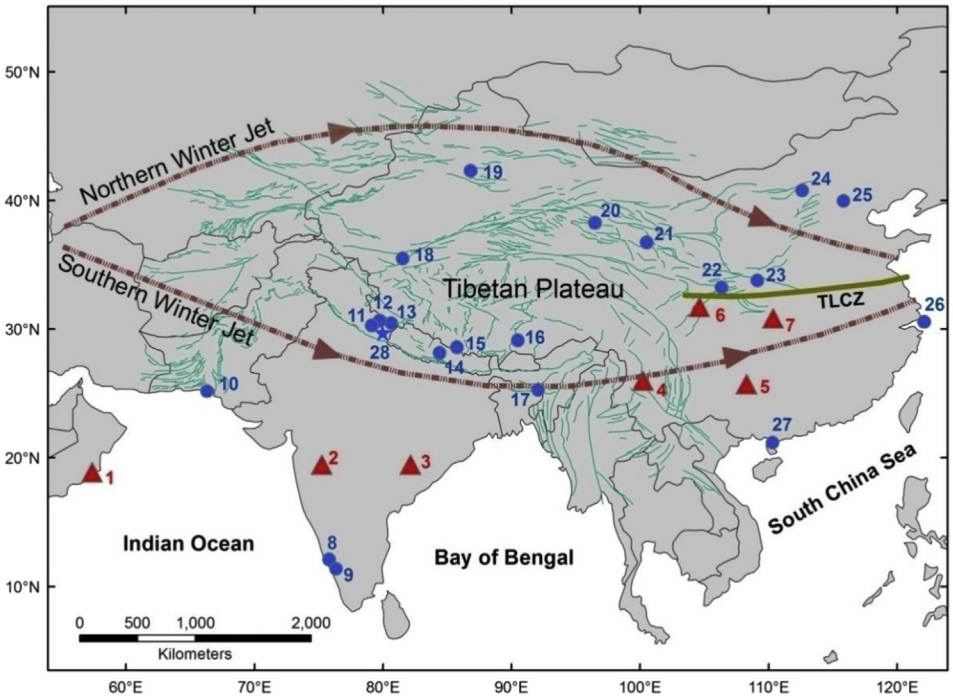

Fig. 1. Location of Panigarh cave and selected sites discussed in the text relative to the Tibetan Plateau and winter jet streams. Red triangles (blue circles) show sites with evidence of drier (wetter) conditions during the LIA. TLCZ is the Tibetan Lee Convergence Zone where the northern and southern winter jets converge. 1) Marine core RC2735/RC2730 (Anderson et al., 2002); 2) Rivers in central and western India (Kale and Baker, 2006); 3) Dandak and Jhumar caves (Yadava and Ramesh, 2005; Sinha et al., 2007, 2011); 4) Lake Erhai (Chen et al., 2005); 5) Dongge cave (Wang et al., 2005); 6) Wanxiang cave (Zhang et al., 2008); 7) Heshang cave (Hu et al., 2008); 8) Akalagavi cave (Yadava et al., 2004); 9) Kerala, Western Ghat (Borgaonkar et al., 2010); 10) Marine core 56KA/39KG (von Rad et al., 1999); 11) Sainji cave (Kotlia et al., 2014); 12) Chularasim Cave (Kotlia et al., 2012); 13) Pinder Valley (Rühland et al., 2006); 14) Siddha Baba Cave (Denniston et al., 2000); 15) Dasuopu ice cap (Thompson et al., 2000); 16) Chencuo (Yang et al., 2004); 17) WahShikar cave (Sinha et al., 2011); 18) Guliya ice cap (Yao et al., 1996); 19) Lake Bosten (Chen et al., 2006); 20) Dunde ice cap (Liu et al., 1998); 21) Lake Qinghai (Zhang et al., 2003); 22) Dayu cave (Tan et al., 2009); 23) Buddha cave (Paulsen et al., 2003); 24) Lake Daihai (Jin et al., 2001); 25) Shihua cave (Ku and Li, 1998); 26) Changjiang prodelta (Yi et al., 2006); 27) Lake Huguanyan (Chu et al., 2002); 28) Dharamjali cave (Sanwal et al., 2013). Star indicates Panigarh cave (this study). (For interpretation of the references to color in this figure legend, the reader is referred to the web version of this article.)

PGH-1 stalagmite consists of both calcite and aragonite, but includes upper and lower sections dominated by the latter, $\delta^{18}O$ and $\delta^{13}C$ values were determined with respect to aragonite. Isotopic values for samples drilled from the central calcite-rich zone of PGH-1 were corrected for percent calcite determined by XRD analysis. Calcite varied from 20 to 100% of the sample. Assuming that the calcite in each sample was deposited with +1.0‰ and +1.7‰ $\delta^{18}O$ and $\delta^{13}C$, respectively, with respect to the aragonite in the sample, an adjusted "all aragonite" value was estimated and reported in this study.

Twelve finely powdered subsamples (sectioned 1 cm interval) of stalagmite were subjected to selected major and trace elements investigation. The concentrations of 19 elements (Al, Ba, Br, Ca, Cl, Cr, Cu, Fe, K, Mg, Mn, Na, P, S, Si, Sr, Ti, V and Zn) were measured using an X-ray fluorescence (XRF) spectrometer (Model: Rigaku RIX2000) equipped with an Rh tube, as described in Selvaraj et al. (2010). About 2–3 g of each powdered sample was compacted into a round disc (30 mm diameter) under appropriate pressure with cellulose as the backing. These pellets were X-rayed and the measurements were carried out at acceleration voltage of 50 kV and a current of 50 mA. The accuracy of the analytical method was established with the standard reference materials (SRMs) MAG-1, BCSS-1, PACS-1, NIES-2 and GBW 07314. Based on the analyses of SRMs, accuracy of the analysis were within ±5% for Al, Br, Ca, Cl, Cr, Fe, K, Mg, Si, Sr, Ti and Zn and within ±10% for Ba, Cu, Mn, Na, P, S and V.

4. Chronology

The five ICP-MS U-series ages for the PGH-1 stalagmite are all in stratigraphic order and were used to construct a chronology for the stalagmite. The ages ranged from 9 ± 34 yr BP at 6 mm to 725 ± 9 yr

Table 1
Mean climate statistics for Pithoragarh and Mukteshwar (after Kotlia et al., 2000). Pithoragarh is 9 km NW whereas Mukteshwar is about 140 km SW of Panigarh cave.

Variable	Jan	Feb	Mar	Apr	May	Jun	Jul	Aug	Sep	Oct	Nov	Dec	Ann
Pithoragarh (29.58°N, 80.21°E; precipitation 1998–2004; temperature 1975–1980)													
Mean precip. (mm)	34.6	63.0	43.5	51.6	122.3	164.9	299.3	276.1	162.1	30.5	3.9	5.5	1257.2
Minimum precip. (mm)	4	0	0	0.5	54.5	76.2	206.2	197.6	102.3	20.8	2.3	0.9	807.0
Maximum precip. (mm)	77	168.5	95.2	132.9	217.7	342.8	495.0	453.8	217.9	110.0	9.7	27.8	1627.4
Mean monthly temp. (°C)	7.7	9.8	13.8	18.2	22.0	23.6	23.3	23.3	22.5	20.2	15.5	8.8	17.4
Mukteshwar (29.47°N, 79.65°E; precipitation 1897–2000; temperature 1897–2004)													
Mean precip. (mm)	54.7	57.6	52.6	39.3	61.8	163.4	311.7	299.0	1959.0	53.0	11.7	24.1	1324.8
Minimum precip. (mm)	0	0	0	0	20	180	780	830	140	0	0	0	694
Maximum precip. (mm)	247	197	210	343	342	607	748	631	613	477	3434	1170	2255
Mean monthly temp. (°C)	6.1	6.9	10.9	15.4	18.1	18.8	17.6	17.1	16.4	14.3	11.0	8.2	13.4

BP at 140 mm from the top of the stalagmite (Table 2; Fig. 2). The age of the top layer of the stalagmite was assumed to be AD 2005 as the stalagmite was active when collected in January 2006. The age of 9 ± 34years for carbonate at 6 mm strongly suggests that the stalagmite was active in 2006 as we observed. This age was not used in developing a chronology due to the relatively large uncertainty associated with it. The chronology developed indicates that stalagmite PGH-1 grew over a period of ~750 years from AD 1256–2005.

The chronology for PGH-1 assumes constant but different accumulation rates in the basal aragonite (97–145 mm depth), middle calcite/aragonite (33–97 mm depth), and upper aragonite (0–33 mm depth) sections of the deposit (Fig. 2). Ages for samples from each zone were determined using linear regression. The relationship for the upper zone suggests an age of 61 calendar years BP (cal BP) or AD 1889 for the boundary between aragonite and calcite at 33 mm depth. The relationship for the basal zone indicates an age of 694 cal BP (AD 1256) for the very base of the stalagmite at 145 mm and an age of 461cal BP (AD 1489) for the calcite–aragonite boundary at 97 mm. An age equation for the middle zone was obtained by regressing the U-series age of 348 ± 91 yr and the two extrapolated ages for the upper and lower boundaries of the calcite/aragonite zone (61 and 461 cal BP).

PGH-1 grew at 0.21 mm/yr from 145 to 97 mm, 0.16 mm/yr from 97 to 33 mm, and 0.28 mm/yr from 33 mm to the top of the stalagmite. These different rates suggest relatively slower vertical growth from AD 1489 to 1889, during a period that may conform to the LIA in the western Himalayan foothills.

5. Petrography

The upper 33 mm and the basal 48 mm of the PGH-1 stalagmite consist entirely of aragonite. In contrast, the middle section from 97 to 33 mm from the top is dominated by calcite containing several lesser bands of aragonite (Figs. 2–4).

5.1. Lower section of the stalagmite

The basal 48 mm consists entirely of elongate bundles of aragonite needles. Individual crystals of this aragonite are typically up to 0.08 mm long and 0.005 mm wide. The aragonite alternates between two fabrics. One is a frothy or spongy aragonite with pores separating aragonite needle bundles (Fig. 4A). It is present from 145 to 130 mm and from 117 to 112 mm from the top of the stalagmite. The presence of relatively high concentrations of Si, Al, and Fe in this aragonite (Fig. 5) suggests that it contains significant clay and iron oxides, perhaps in the dark tops of the bundles of aragonite crystals. However, individual particles or clusters of clay and Fe oxide are not visible via light microscopy, suggesting that it is present only in tiny particles that may have reached to stalagmite as airborne dust. The frothy or spongy aragonite is also distinct in having relatively high concentrations of P and S, which are presumably present as PO_4^{3-} and SO_4^{2-} substituting for CO_3^{2-}. Because these are trace ions with low distribution coefficients in carbonate minerals, and because low distribution coefficients commonly increase with increasing precipitation rate (Railsback, 1999), the presence of these ions in the highest concentrations found in the stalagmite suggests faster carbonate precipitation. The frothy or spongy aragonite is also distinct among the stalagmite's aragonite intervals in having the lowest Sr concentrations (Fig. 5). Because Sr^{2+} has a large distribution coefficient in aragonite and because large distribution coefficients typically decrease with increasing precipitation rate (Railsback, 1999), this pattern likewise suggests faster precipitation of the spongy aragonite. According to Fairchild et al. (2001), Mg in stalagmite is sensitive to hydrology, Sr and Na are influenced by growth rate, and P may be the most sensitive proxy for seasonal temperature changes. All these observations (frothy aragonite suggestive of fast precipitation, windborne dust, and P, S, and Sr concentrations suggestive of fast precipitation) suggest formation of this aragonite under relatively dry conditions.

The other fabric of aragonite in the lower third of the stalagmite consists of dense aragonite with few voids (Fig. 4B, orange (in the web version) shading). This dense aragonite is banded at intervals of about 0.2 mm. Given the entire stalagmite's history of 145 mm deposited over 750 years and thus an average depositional rate of 0.20 mm per year, these bands are likely annual. This dense aragonite is present in the intervals from 130 to 117 mm and from 112 to 97 mm from the top of the stalagmite.

5.2. Middle section of the stalagmite

The middle section of the stalagmite (from 97 to 33 mm from the top), is dominated by porous calcite consisting of near-vertical columnar crystals up to 0.75 mm wide and as much as 2.2 mm long. In addition to this calcite, there are at least 16 aragonite layers in this interval that vary in thickness from 0.2 to 2 mm (Fig. 4C). These aragonite layers are thinner and usually discontinuous near the central growth axis and become thicker and more continuous outward. In the interval from 57 to 33 mm from the top of the stalagmite, layers commonly change from calcite along the stalagmite's growth axis to dense aragonite on the stalagmite's flank. This pattern of calcite in the central zones of stalagmite layers and aragonite on the flanks has been observed elsewhere (e.g., Railsback et al., 1994) and is commonly attributed to more extensive modification of drip water by evaporation as the water moves across the stalagmite (Mills, 1965).

Table 2
Uranium-series age data for the PGH-1 stalagmite.

Sample ID	Depth (cm)	^{238}U (ppb)	^{232}Th (ppt)	[^{230}Th/^{232}Th] (ppm)[a]	δ^{234}U measured[b]	[^{230}Th/^{238}U] Activity	^{230}Th age uncorrected[c]	$\delta^{234}U_{initial}$ corrected[d]	^{230}Th age corrected[e]	^{230}Th age corrected (yr AD)[f]
HMS-1	0.5	3214.5 ± 150.8	13,421.7 ± 630.7	5.2 ± 0.4	1528.2 ± 3.8	0.00131 ± 0.00009	57 ± 4	1528 ± 3.8	9 ± 34	1998 ± 34
HMS-2	2.5	3510.0 ± 5.3	4027.4 ± 12.4	34.7 ± 1.0	1614.3 ± 3.3	0.00241 ± 0.00007	101 ± 3	1614 ± 3.3	88 ± 7	1919 ± 7
HMS-3	7.0	284.3 ± 13.3	2893.1 ± 134.8	17.4 ± 1.4	1521.8 ± 16.6	0.01072 ± 0.00088	465 ± 38	1523.3 ± 16.6	348 ± 91	1659 ± 91
HMS-4	11.0	2513.1 ± 3.6	2815.6 ± 10.3	206.9 ± 2.6	1598.1 ± 3.4	0.01407 ± 0.00017	591 ± 7	1600.7 ± 3.4	579 ± 10	1428 ± 10
HMS-5	14.0	3319.3 ± 185.8	11,232.6 ± 630.6	91.1 ± 1.5	1685.2 ± 4.6	0.01868 ± 0.00030	762 ± 12	1688.7 ± 4.7	725 ± 29	1282 ± 29

[a] The degree of detrital ^{230}Th contamination is indicated by the [^{230}Th/^{232}Th] atomic ratio instead of the activity ratio.
[b] $\delta^{234}U = ([^{234}U/^{238}U]$ activity $- 1) \times 1000$.
[c] Analytical errors are 2σ. Decay constants are 9.1577×10^{-6} yr^{-1} for ^{230}Th, 2.8263×10^{-6} yr^{-1} for ^{234}U and 1.55125×10^{-10} yr^{-1} for ^{238}U (Cheng et al., 2000).
[d] $\delta^{234}U_{initial}$ was calculated based on ^{230}Th age (T), i.e., $\delta^{234}U_{initial} = \delta^{234}U_{measured} \times e^{\lambda 234 \times T}$.
[e] Age corrections were calculated using an average crustal ^{230}Th/^{232}Th atomic ratio of $4.4 \times 10^{-6} \pm 2.2 \times 10^{-6}$. Those are the values for a material in secular equilibrium with the crustal ^{232}Th/^{238}U value of 3.8. The errors are arbitrarily assumed to be 50%.
[f] The samples were dated in 2007 so the corrected^{230}Th age was subtracted from 2007 to obtain ages in years AD.

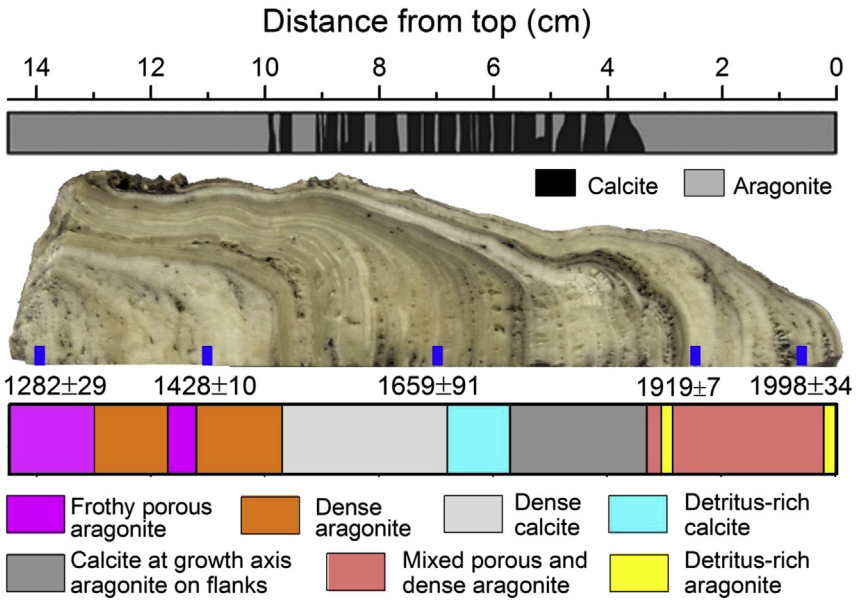

Fig. 2. Section through the 14.5 cm long Panigarh cave stalagmite PGH-1 showing calcite–aragonite stratigraphy, locations of dated samples, and U-series ages in years AD.

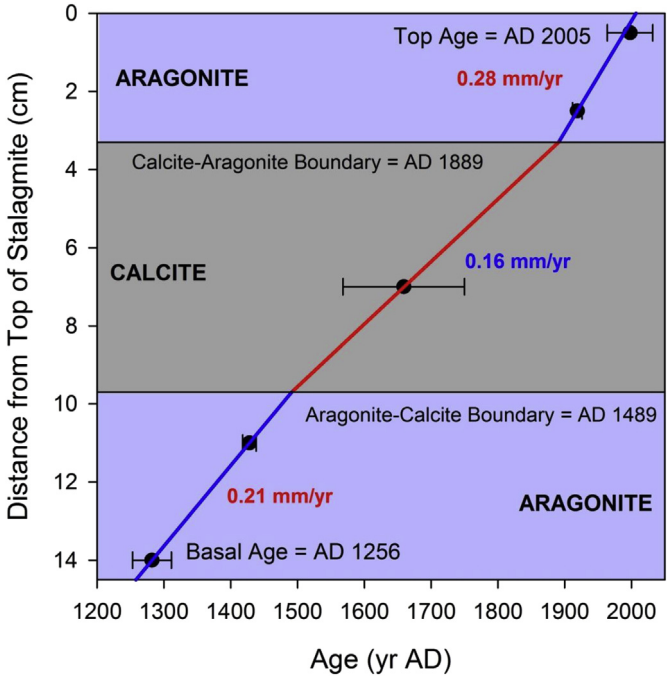

Fig. 3. U-series age–depth data for the PGH-1 stalagmite showing growth rates in the calcite and aragonite sections of the deposit. The age at the top of the stalagmite is assumed to be AD 2005 as the stalagmite was active when collected in January 2006. Separate age relationships were calculated for the three major zones of the stalagmite: 1) upper aragonite zone, 2) middle calcite zone, and 3) lower aragonite zone. Age estimates at the boundaries between aragonite and calcite using the three models are shown. Growth rates in each zone are indicated. Equations are: basal aragonite: Age (yr) = 1962 − 4.87*(Depth in mm); middle calcite: Age (yr) = 2095 − 6.24*(Depth in mm); and upper aragonite: Age (yr) = 2009 − 3.64*(Depth in mm).

5.3. Upper section of the stalagmite

The uppermost 33 mm of the stalagmite is mainly aragonite, with crystals up to 0.005 mm wide and 0.5 mm long. Like the lowest 48 mm of the stalagmite, this uppermost interval varies between porous zones consisting of large bundles of aragonite and dense zones of layered aragonite. However, whereas the lowest 48 mm can be divided into separate intervals of each fabric, the uppermost 33 mm consist of intergrading fabrics.

5.4. Layers of non-carbonate detrital material

Three intervals of the stalagmite are characterized by thin layers of non-carbonate detrital material. In the interval from 57 to 68 mm from top of the stalagmite, there are four distinct layers that contain gray–brown, non-carbonate detrital material. The color and texture of this material suggest a mixture of clays and Fe oxides. These layers are as much as 0.08 mm thick and are thickest near the crest of the stalagmite; they are found at the tops of both aragonite and calcite layers. At the top of one such layer is a discrete grain of the same material that is 0.14 mm in diameter. Secondly, in the interval from 28.5 to 30.5 mm from the top of the stalagmite, there are four layers of a similar very fine gray–brown material capping layers of aragonite. Amidst this material are detrital tectosilicate (quartz or feldspar) grains as much as 0.15 mm in diameter and thus in the size range of fine sand. Finally, thin layers of this detrital material cap layers of aragonite in the uppermost 2 mm of the stalagmite (Fig. 4D).

Detrital non-carbonate material in stalagmite can be deposited as wind-blown dust that settles onto the stalagmite surface (as noted above) and as water-borne grains deposited on the stalagmite's surface by drip water. In wind-blown material, no sand-size grains are expected unless the stalagmite has formed at the mouth of a cave in a desert region, and the detrital layer may thin at the stalagmite's crest because detrital material was washed away by drip water (e.g. Webster et al., 2007). In water-borne sediment, the detrital material may include silt-sized or sand-sized grains, and its deposition from drip water may lead to thicker accumulation near the crest of the stalagmite. These considerations suggest that the recognizable layers of detrital material in the upper two thirds of PGH-1 were deposited by flushing water and thus represent episodic wetter conditions.

5.5. General inferences from the mineralogy of stalagmite PGH-1

Microscope petrographic study revealed no Type L or Type E layers (see Railsback et al., 2011) in the thin sections, indicating

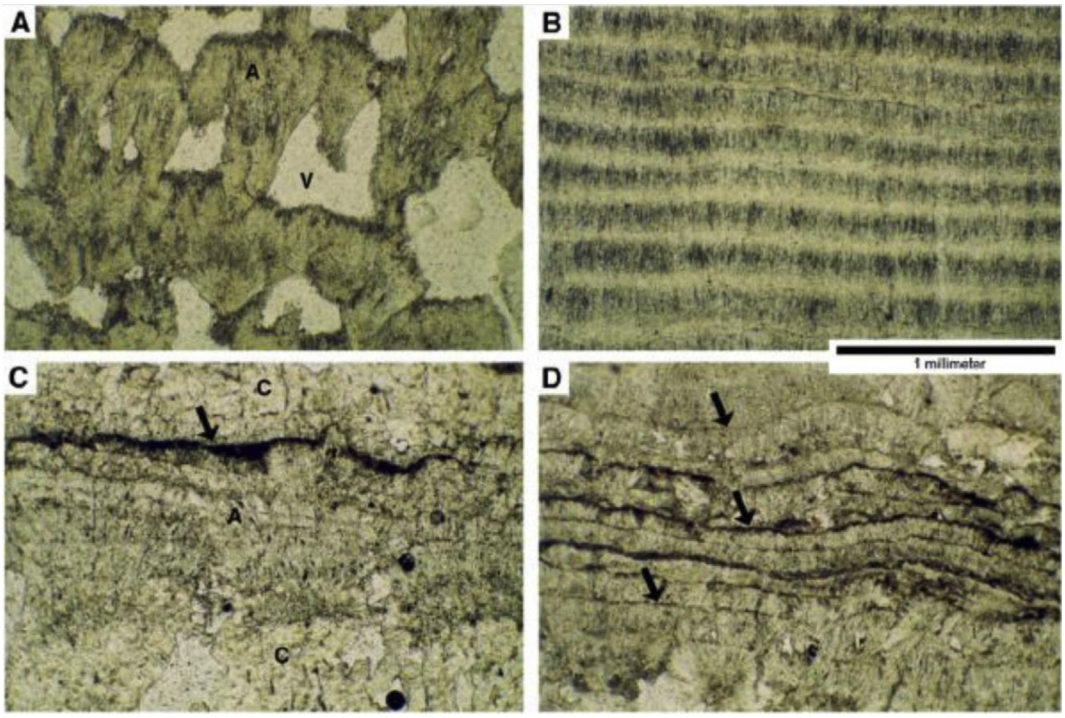

Fig. 4. Photomicrographs of stalagmite PGH-1 in plane-polarized transmitted light. The scale is the same for all four images. A. Bundles of aragonite (A) and void space (V) in a frothy or spongy interval of aragonite in the lower third of the stalagmite. B. Layers of dense aragonite in lower third of stalagmite. The thickness of these layers is compatible with deposition of one per year, as discussed in text. C. Part of middle third of stalagmite in which calcite (C) is overlain by aragonite (A) that is capped by a layer of non-carbonate detrital material (arrow) that is overlain by calcite (C). D. Layers of aragonite in the uppermost 0.2 cm of the stalagmite, with thin layers of non-carbonate detrital material (arrows).

continuous deposition of the stalagmite. Alternating deposition of aragonite and calcite can be interpreted in at least two ways. Aragonite is commonly associated with drier conditions and greater evaporation, and calcite with wetter conditions and less evaporation, and thus a lower saturation state (Murray, 1954; Siegel, 1965; Siegel and Dort, 1966; Thrailkill, 1971; Reams, 1972; Cabrol and Coudray, 1982; Railsback et al., 1994). On the other hand, aragonite is known to be favored by precipitation at higher temperatures and calcite by precipitation at lower temperatures (Burton and Walter, 1987). Coincidence of the calcitic phase of stalagmite deposition with much of the LIA suggests that temperature may have been a significant control on overall changes in mineralogy of PGH-1. However, the lateral transition from calcite to aragonite along layers in the more generally calcitic middle part of the stalagmite suggests that conditions were relatively dry, even when calcite was precipitated at the crest of the stalagmite. In addition, the presence of water-borne detrital material on the upper surfaces of aragonite layers suggests that intervals of aragonite were at least punctuated by periods of considerable flow of water onto the stalagmite.

6. Color and luminescence

Luminescence along the central growth axis of PGH-1 ranges from 110 to 230 with higher values indicating stronger luminescence (Fig. 6E). There is no long-term trend in luminescence although frothy aragonite at 145–130 mm has lower luminescence than less porous calcite or compact aragonite in the upper 130 mm of PGH-1. Where detrital material with low luminescence is present, overall luminescence drops (vanBeynen et al., 2001). Luminescence is also lower when pores and cavities are present in the carbonate.

Stronger luminescence can result from an increase in organic acids within the carbonate or in fluid inclusions (Lauritzen et al., 1986; Shopov et al., 1994; Ramseyer et al., 1997), either in the form of humic or fulvic acids (vanBeynen et al., 2001). These organic acids are produced in the soil by plants and are then transported into the cave by percolating waters and may eventually become sealed in fluid inclusions in stalagmite carbonate. Increased plant activity at the surface (usually under warmer and wetter conditions) produces more organic acids that can be transported into the cave. Under a warmer climate, humic acids are broken down by bacteria in the soil to form fulvic acids (Lauritzen et al., 1986; Shopov et al., 1994). Thus, increased luminescence, particularly associated with lighter colors, indicating the presence offulvic acids that are colorless, suggests a warmer/wetter climate, while lower luminescence coupled with darker colors indicates a cooler/drier climate. Drier conditions limit plant growth and hence the production of organic acids. This may be why spongy aragonite deposited at 145–130 mm has relatively low luminescence and the upper 10 mm of the stalagmite, containing cavities, has extremely low luminescence. Therefore, we assume that increased luminescence of the PGH-1 stalagmite carbonate is a proxy for warmer/wetter conditions while lower luminescence indicates cooler/drier conditions.

Reflective color of the PGH-1 stalagmite varies considerably. Generally, aragonite in the basal 48 mm and upper 33 mm has higher values (brighter in color) and calcite in the central section of the deposit at 97–33 mm is slightly darker in color (Fig. 6E). Superimposed on this broad pattern are high-frequency variations, with more-porous calcite/aragonite being darker, and more compact calcite/aragonite appearing lighter in color. Layers with detrital material are much darker while clean aragonite and calcite are much whiter. In addition, high-frequency fluctuations in luminescence and color along the central growth axis of PGH-1 broadly parallel one another.

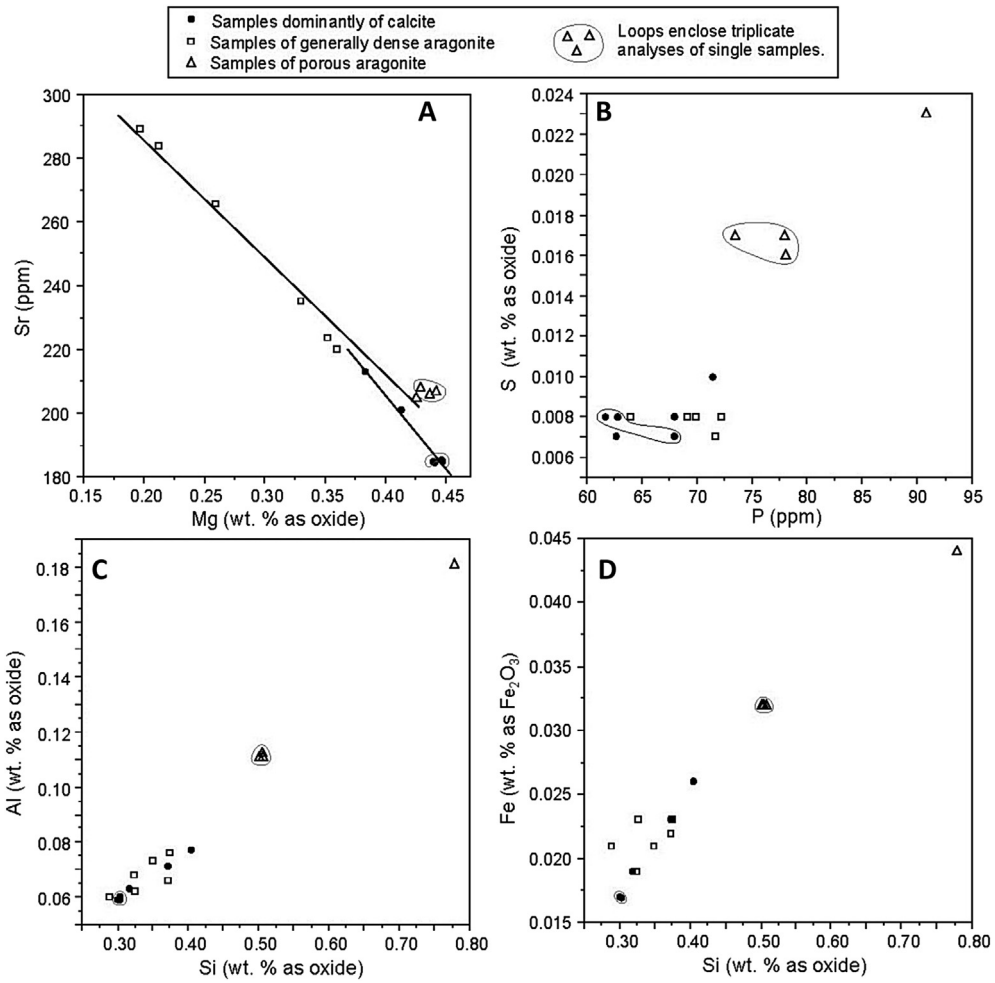

Fig. 5. Concentrations of minor and trace elements in stalagmite PGH-1. Open symbols indicate samples from aragonitic intervals, and filled symbols indicate samples from calcitic intervals. A. Inverse correlation of Mg and Sr, which is expected in samples ranging from purely aragonite (where Sr is typically more abundant) to purely calcite (where Mg is typically more abundant). B. Positive correlation of P and S, presumably present as PO_4^{3-} and SO_4^{2-} substituting for CO_3^{2-}. C and D. Positive correlation of Al and Fe with Si, suggesting that the three co-occur as clays and Fe oxides in detrital non-carbonate material.

7. Stable isotopes

Along the central growth axis $\delta^{18}O$ and $\delta^{13}C$ values, normalized to an all-aragonite basis, range from −8.3‰ to −5.1‰ (VPDB) and −8.7‰ to −3.1‰ (VPDB) respectively. $\delta^{18}O$ and $\delta^{13}C$ values show larger amplitude of fluctuations in the upper and lower aragonite-dominated sections than the central calcite-dominated section (Fig. 6E), possibly indicating significant climate shifts at the beginning and end of the LIA in northern India.

The shallow nature of the cave and the considerable seasonal and diurnal variations in temperature lead us to assume that kinetic effects must have influenced the final isotopic composition of the stalagmite. In general, when stalagmite carbonate is deposited under the influence of evaporation and rapid degassing of CO_2, $\delta^{18}O$ and $\delta^{13}C$ values tend to be enriched in the heavy isotopes compared to those deposited under isotopic equilibrium conditions, and more so under increasingly evaporative conditions (Hendy, 1971).

The $\delta^{18}O$ of stalagmite carbonate is also influenced by temperature and the $\delta^{18}O$ of the precipitating water. Under warmer conditions, $\delta^{18}O$ values decrease by 0.23‰ per °C (Friedman and O'Neil, 1977). In fact, the mean $\delta^{18}O$ value of carbonate in the calcite zone of PGH-1 (−6.78‰) is lower than the mean values for the upper (−6.65‰) and lower (−6.45‰) aragonite zones. Given that the calcite was deposited during the LIA, it is difficult to explain this in terms of a higher temperature at the time of deposition. This leads to the conclusion that the difference is due to lower $\delta^{18}O$ in the cave dripwaters, which approximates the monthly average value of meteoric rainfall (e.g. Yonge et al., 1985). However, the $\delta^{18}O$ value for meteoric water can be affected by evaporation before reaching the cave and higher temperatures make this more likely. Therefore, it is possible that the lower carbonate $\delta^{18}O$ values during the LIA are due to reduced evaporation of meteoric waters before they reach the cave with higher values during deposition of aragonite when evaporation was probably much higher.

There are two types of precipitation isotope data available for the Panigarh area according to the International Atomic Energy Agency web site (https://www.iaea.org/). A 40-year long record is available for New Delhi, 300 km southwest of Panigarh cave, located on the plains south of the Himalayas at a much lower elevation (212 m versus 1520 m), and there are several short records for stations in the foothills of the Himalayas, in an area extending from 29.40°N to 31°N and 77.89°E to 79.46°E that is close to Panigarh cave and at a broadly similar elevation (Fig. 1). We examined both types of record to determine what climatic factors influence $\delta^{18}O$ of meteoric waters in the area. In addition, there are long instrumental climate records available for the area and we will compare these with our record from PGH-1 for the same time period to seek correlations.

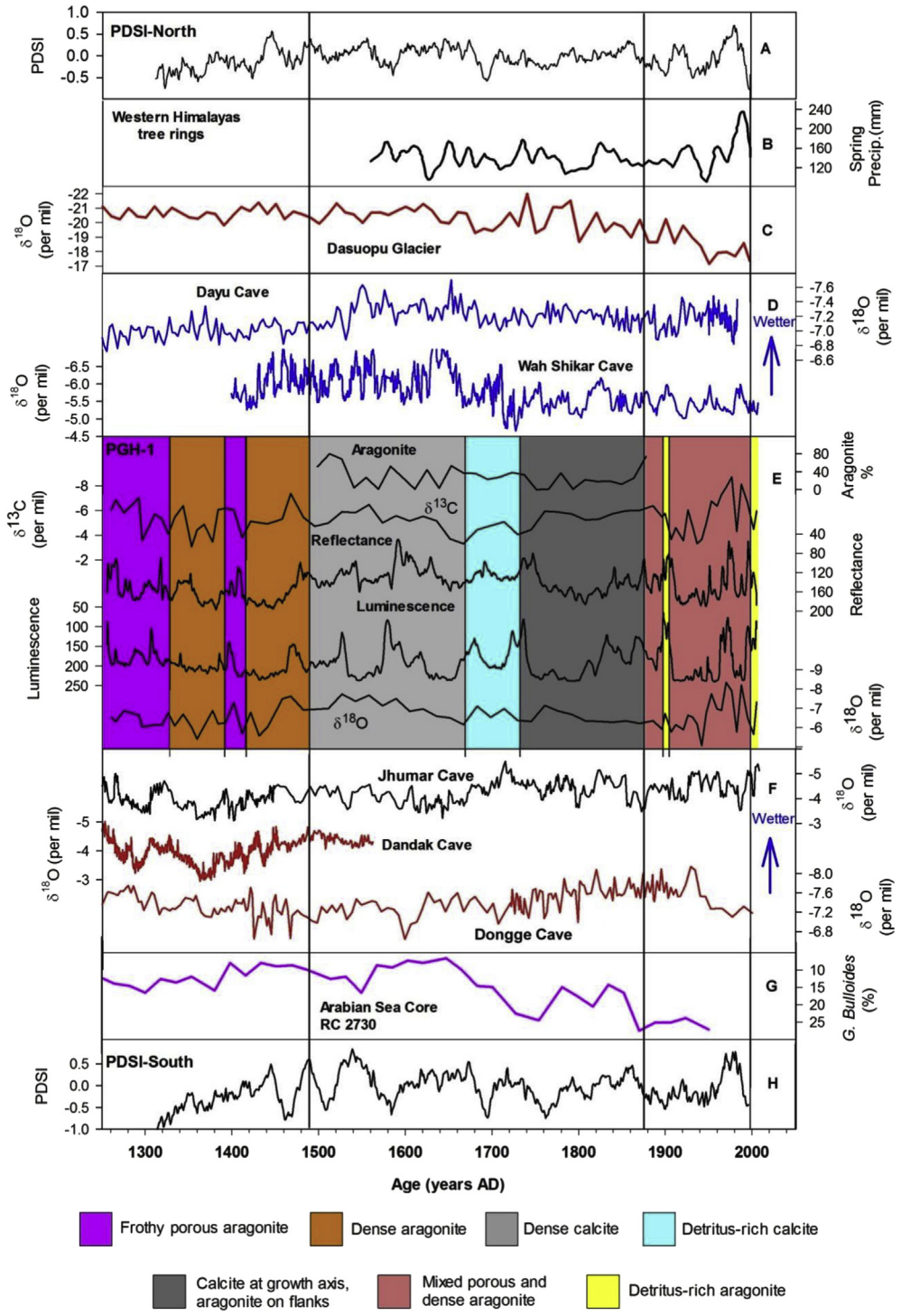

Fig. 6. Comparison of the PGH-1 stalagmite record (E) with records from other sites, as well as Palmer Drought Severity Indices (PDSI) at 28.75°N, 78.75°E (A) and 21.25°N, 78.75°E (H) after Cook et al. (2010). B. Tree ring precipitation record for the western Himalayas. The data were smoothed using a cubic spline designed to remove 50% of the variance in a sine function with a wavelength of 20 years (after Singh et al., 2006); C. Isotope temperature record from the Dasuopu glacier, Tibetan Plateau (Thompson et al., 2000); D. Dayu cave after Tan et al. (2009) and WahShikar cave after Sinha et al. (2011); F. Jhumar and Dandak Caves after Sinha et al. (2007, 2011) and Dongge Cave after Wang et al. (2005); G. Arabian Sea box cores after Anderson et al. (2002).

The annual cycle at New Delhi and at the stations in the foothills of the Himalayas is similar (Figs. 7 and 8C–F). Over the course of a typical year $\delta^{18}O$ values for New Delhi follow a sinusoidal curve with maximum values in April and minimum values in September. Similar patterns are observed at the stations in the mountains with the lowest $\delta^{18}O$ values being associated with heavy monsoon rains in summer and the highest values with lighter rains in the dry season winter months.

At New Delhi, there is no significant relationship between monthly weighted mean $\delta^{18}O$ of precipitation for January–December, and either mean monthly temperature or monthly precipitation amount, or between precipitation amount and

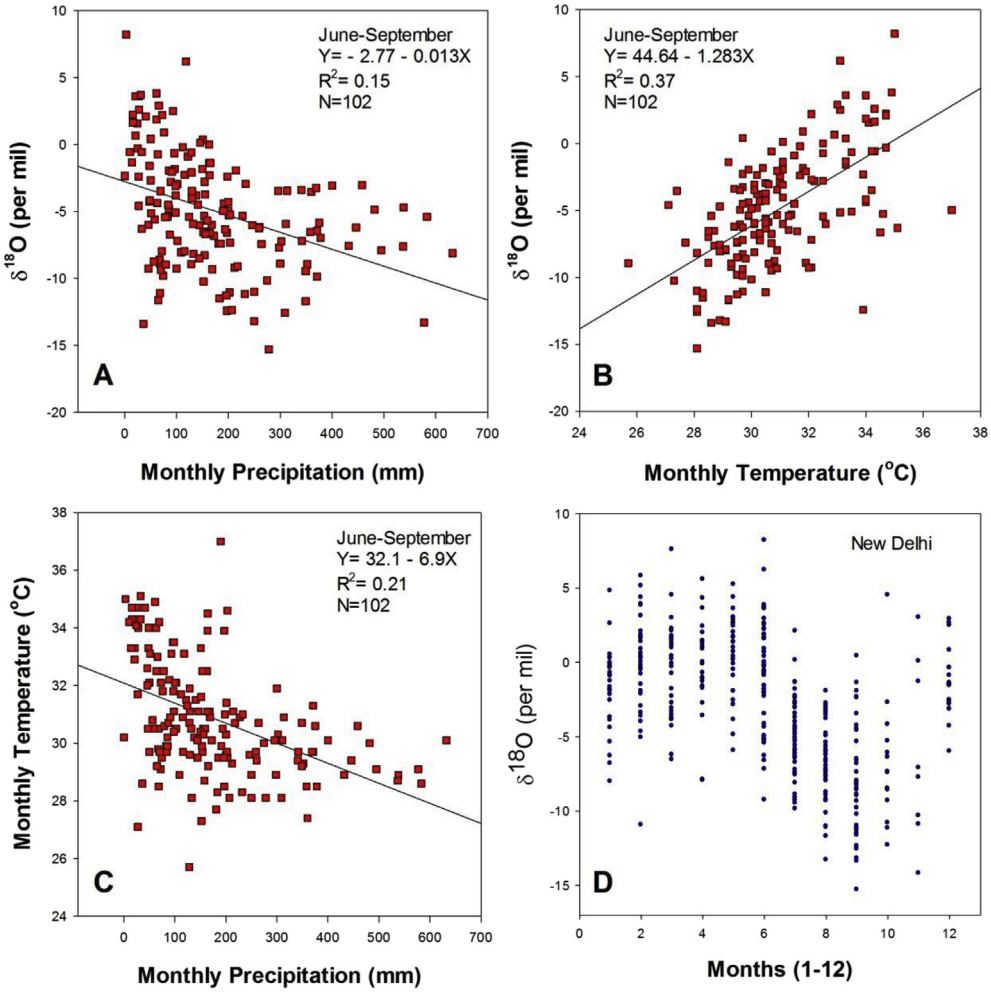

Fig. 7. Relationships among $\delta^{18}O$ of precipitation, precipitation amount, temperature and month of precipitation at New Delhi. A. $\delta^{18}O$ of precipitation and precipitation amount June–September; B. $\delta^{18}O$ of precipitation and mean monthly temperature June–September; C. Precipitation amount and mean monthly temperature June–September; and D. Monthly variations in $\delta^{18}O$ of precipitation January–December. New Delhi is 300 km SW of Panigarh cave.

temperature. In the dry season months of December–March (102 months of data) linear regressions produce R^2 values of 0.10 and 0.05 between $\delta^{18}O$, and precipitation and temperature, respectively, while a regression between temperature and precipitation gave an R^2 of 0.01. These weak relationships show that in the New Delhi area $\delta^{18}O$ increases with increasing temperature and decreases with increasing precipitation. In contrast, during the four monsoon months of June–September, clear relationships are apparent (Fig. 7A–C). $\delta^{18}O$ values decrease with increasing precipitation ($R^2 = 0.15$) and increase with increasing temperature ($R^2 = 0.37$), while there is a negative relationship between precipitation and temperature ($R^2 = 0.21$). This last relationship is clearly caused by the drop in temperature that typically accompanies heavy monsoon rains.

At all but one of the 10 stations (Gomukh) in the mountains, monsoonal July–October monthly $\delta^{18}O$ of precipitation decreased with increasing precipitation amount (Table 3). Only two stations, Uttarkashi and Maneri, had data for the six-month November–April dry period and again $\delta^{18}O$ of precipitation decreased with an increase in precipitation. These data indicate that the $\delta^{18}O$ of rainfall is strongly influenced by the precipitation "amount effect" that has been shown to be an important control in many areas of the world (e.g. Vuille et al., 2005: 7–8). The data we analyzed, some of which are shown in Figs. 7 and 8, suggest that precipitation in the monsoon months of July through October is most depleted in ^{18}O compared with other months of the year. If low values of $\delta^{18}O$ in monsoonal rainfall were transferred to PGH-1, then lower $\delta^{18}O$ values for carbonate in the stalagmite may record periods of higher monsoonal precipitation.

If the isotopic characteristics of monsoonal rainfall are transferred to stalagmites then instrumental data on precipitation amount should parallel isotopic variations in stalagmites. In fact, long-term variations in annual and 5-year mean monsoonal rainfall for all India (Parthasarathy et al., 1995), as well as at Mukteshwar during the last 100 years (AD 1901–2000), close to Panigarh cave, do parallel fluctuations in $\delta^{18}O$ of the upper aragonite zone in PGH-1 (Fig. 9). In particular, high $\delta^{18}O$ values correlate with low monsoon rainfall, and thus lower relative humidity and increased evaporation, during brief periods centered on 1906, 1920, 1940, 1965, 1982, and 2001 (Fig. 9). High $\delta^{18}O$ values during these periods (except the period centered on 1982) also correlate well with low standardized precipitation index (SPI) values (McKee et al., 1993) in the AD 1901–2000 monthly precipitation record (Fig. 9A and F). The lower SPI values reflect moderately-to-severely dry and extremely dry periods according to the classification scheme of McKee et al. (1993). In fact, the high $\delta^{18}O$ values during the period centered at 1982 may correspond to the lower SPI values centered at 1978, considering chronological uncertainties in our records.

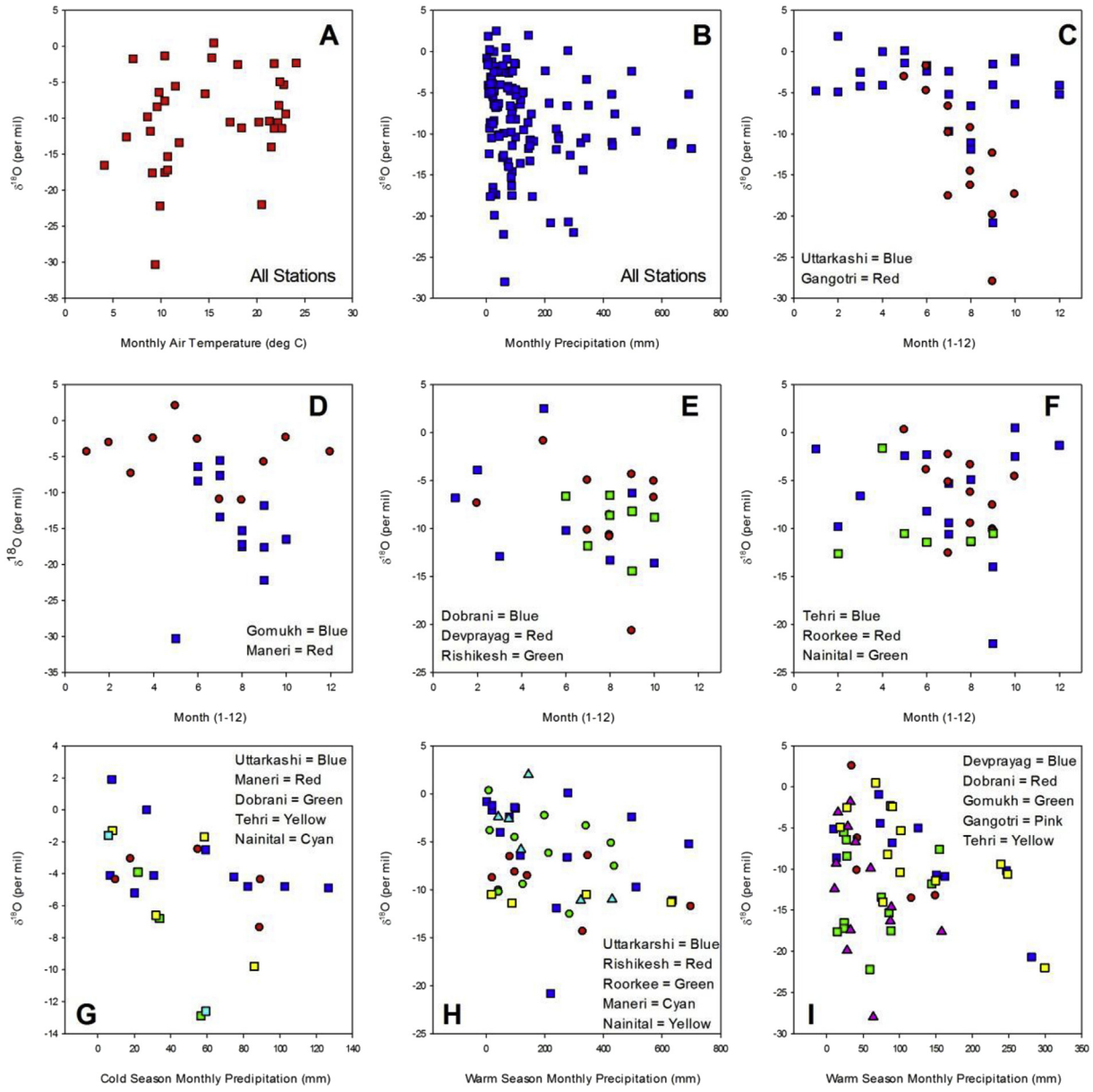

Fig. 8. Precipitation isotope values relative to time of year, precipitation amount, and temperature in stations of the Himalayan foothills. Note that winter is Dec to Feb; Fall Sept to Nov; Spring March to May; Summer June to August (Barry and Chorley, 2003). A. All stations monthly air temperature vs. precipitation $\delta^{18}O$; B. All stations monthly precipitation vs. precipitation $\delta^{18}O$; C. Monthly variation in precipitation $\delta^{18}O$ at stations Uttarkashi and Gangotri; D. Monthly variation in precipitation $\delta^{18}O$ at stations Gomukh and Maneri; E. Monthly variation in precipitation $\delta^{18}O$ at stations Bobrai, Devprayag, and Rishikesh; F. Monthly variation in precipitation $\delta^{18}O$ at stations Tehri, Roorkee, and Nainital; G. Cold season monthly precipitation vs precipitation $\delta^{18}O$ at stations Uttarkashi, Maneri, Dobrani, Tehri, and Nainital; H. Warm season monthly precipitation vs. precipitation $\delta^{18}O$ at stations Uttarkashi, Maneri, Dobrani, Tehri, and Nainital; I. Warm season monthly precipitation vs. precipitation $\delta^{18}O$ at stations Devprayag, Dobrani, Gomukh, Gangotri, and Tehri.

These correlations for the last 100 years suggest that PGH-1 $\delta^{18}O$ values may also be a good proxy for an estimate of deviation from long-term average precipitation over the longer period covered by our records from AD 1256–2005. Yadava and Ramesh (2005) have also shown a clear decrease in $\delta^{18}O$ with increasing monthly rainfall ($r = 0.94$) during July, August and September in 1999.

The rainfall amount effect observed in northern India under sub-tropical climatic conditions influences the $\delta^{18}O$ of stalagmite carbonate in a very similar way to kinetic fractionation. This is because higher rainfall is associated with lower $\delta^{18}O$ while at the same time higher rainfall leads to higher humidities and reduced evaporation that minimize kinetic fractionation, thus maintaining the low values. During dry periods of lower rainfall, such as during the months preceding the onset of the monsoon (Fig. 7D), $\delta^{18}O$ will be higher and humidities lower so that increased evaporation of the rainfall and of water on the stalagmite increases $\delta^{18}O$. Cool periods with low rainfall, and low evaporation because of the cool conditions, will also result in lower $\delta^{18}O$ values in meteoric waters but not as low as during the warm, wetintervals. Thus we interpret low $\delta^{18}O$ values for meteoric water as evidence of very wet monsoonal conditions and higher values as evidence of warm dry conditions. Cool, dry conditions probably produce intermediate meteoric water $\delta^{18}O$ values due to average $\delta^{18}O$ values for rain and low evaporation rates that maintain these original values.

However, approximately 20% of precipitation at Panigarh cave is not associated with the ISM, and it is possible that during the LIA,

Table 3
Regression relationships for climate stations in northern India near Panigarh cave.

Location	Latitude; longitude (degrees)	Period of record	Analysis period	Equation[a]	R^2	N
New Delhi						
New Delhi (300 km SW; 212 m)	28.58N; 77.2E	1/1960–12/2008	Jun–Sept	$\delta^{18}O = -2.768 - 0.013$ (P)	0.15	102
New Delhi (300 km SW; 212 m)	28.58N; 77.2E	1/1960–12/2008	Jun–Sept	$\delta^{18}O = -44.643 + 1.284$ (T)	0.37	102
New Delhi (300 km SW; 212 m)	28.58N; 77.2E	1/1960–12/2008	Jun–Sept	T = 32.084–6.951 (P)	0.21	102
New Delhi (300 km SW; 212 m)	28.58N; 77.2E	1/1960–12/2008	Dec–Mar	$\delta^{18}O = 0.398–0.055$ (P)	0.10	102
New Delhi (300 km SW; 212 m)	28.58N; 77.2E	1/1960–12/2008	Dec–Mar	$\delta^{18}O = -4.680 + 0.221$ (T)	0.05	102
New Delhi (300 km SW; 212 m)	28.58N; 77.2E	1/1960–12/2008	Dec–Mar	T = 17.828 − 0.020 (P)	0.01	102
Stations in the Himalayan foothills						
Uttarkashi (207 km NW; 1140 m)	30.73N; 78.45E	1/2004–12/2006	Nov–Apr	$\delta^{18}O = -1.708 - 0.029$ (P)	0.26	10
Maneri (209 km NW; 1150 m)	30.74N; 78.45E	1/2005–12/2006	Nov–Apr	$\delta^{18}O = -2.987 - 0.026$ (P)	0.27	5
Maneri (209 km NW; 1150 m)	30.74N; 78.45E	1/2005–12/2006	Jul–Oct	$\delta^{18}O = -2.400 - 0.023$ (P)	0.91	4
Uttarkashi (207 km NW; 1140 m)	30.73N; 78.45E	1/2004–12/2006	Jul–Oct	$\delta^{18}O = -3.375 - 8.595$ (P)	0.12	16
Rishikesh (186 km WNW; 356 m)	30.11N; 78.30E	1/2005–12/2006	Jul–Oct	$\delta^{18}O = -7.735 - 6.215$ (P)	0.26	7
Roorkee (218 km WNW; 274 m)	29.87N; 77.89E	1/2003–12/2006	Jul–Oct	$\delta^{18}O = -5.879 - 2.197$ (P)	0.008	12
Nainital (66 km ENE; 1953 m)	29.40N; 79.46E	1/1995–12/1995	Jul–Oct	$\delta^{18}O = -10.778 - 5.441$ (P)	0.09	4
Gangotri (196 km NW; 3053 m)	31.00N; 78.94E	1/2004–12/2006	Jul–Oct	$\delta^{18}O = -8.575 - 0.076$ (P)	0.18	13
Devprayag (161 km WNW; 465 m)	30.14N; 78.60E	1/2004–12/2006	Jul–Oct	$\delta^{18}O = -2.835 - 0.045$ (P)	0.56	10
Dobrani (207 km NW; 2050 m)	30.95N; 78.69E	1/2004–12/2006	Jul–Oct	$\delta^{18}O = -0.958 - 0.093$ (P)	0.54	5
Tehri (181 km WNW; 640 m)	30.35N; 78.48E	1/2004–12/2006	Jul–Oct	$\delta^{18}O = -1.901 - 0.049$ (P)	0.50	13
Gomukh (190 km NW; 3800 m)	30.93N; 78.94E	1/2004–12/2006	Jul–Oct	$\delta^{18}O = -13.797 + 0.011$ (P)	0.01	12

[a] $\delta^{18}O$ is the monthly weighted mean for precipitation (‰); P is monthly precipitation amount (mm); T is mean monthly temperature (°C).

there were changes in the amount of summer versus fall/winter/spring rainfall received at Panigarh cave. Inspection of Fig. 7D, showing monthly $\delta^{18}O$ values at New Delhi, shows that December–May (winter and spring) precipitation generally has higher $\delta^{18}O$ values (>−5‰) than summer and fall (June–November) precipitation, which can reach values as low as ~−15‰. Similarly, $\delta^{18}O$ values for winter/spring precipitation at stations in the foothills of the Himalayas are either higher or comparable to summer/fall $\delta^{18}O$ values (Fig. 8D, E and F). This makes it very difficult to determine if an increase in winter/spring precipitation produced the lower $\delta^{18}O$ values of calcite in the Panigarh stalagmite. Lower values could result from reduced evaporation of meteoric waters or an increase in summer/fall precipitation also.

Stalagmite carbonate $\delta^{13}C$ is influenced by the $\delta^{13}C$ of CO_2 in the soil above the cave, the amount of CO_2 available in the soil, hydrological conditions at the time of limestone dissolution, and the degree of kinetic fractionation of carbon isotopes in the precipitating water (Brook et al., 2006; Webster et al., 2007 and references therein). The $\delta^{13}C$ of soil CO_2 is mainly dependent on the vegetation cover above the cave, with lower values where the plant cover is predominantly of the C_3 type and higher values when C_4 plants predominate. At present, the vegetation near Panigarh cave consists mainly of C_3 plants and it is unlikely that the vegetation changed substantially during the last millennium. However, drier conditions in the past would have enhanced evaporation, restricted plant growth, and reduced the volume of CO_2 in the soil above the cave. Stalagmite carbonate deposited under such conditions would have higher $\delta^{13}C$ values, as more carbon would come from the limestone ($\delta^{13}C$ = 0‰) rather than soil CO_2 ($\delta^{13}C$ of C_3 plants = −27‰) due to the low levels of soil CO_2 and the likelihood that dissolution would be more closed-system than open-system due to limited exchange between carbon dissolved in water from the limestone and carbon in the soil CO_2.

In contrast, stalagmite carbonate with lower $\delta^{13}C$ values would be deposited under wetter conditions, because reduced evaporation allows more plant growth and thus a higher volume of CO_2 in the soil. Increased plant activity and higher production of soil CO_2 would lead to an increase in open-system dissolution of the limestone, which would allow more exchange of carbon derived from dissolution of the bedrock with carbon in the soil CO_2. Thus, higher $\delta^{13}C$ values in the PGH-1 stalagmite should indicate drier/warmer conditions, while lower values should point to wetter/cooler conditions in the Panigarh cave area. This interpretation is supported by the relationship between variations in monsoon rainfall and $\delta^{13}C$ values of speleothem aragonite during the past 100 years with higher $\delta^{13}C$ corresponding to higher $\delta^{18}O$ values in PGH-1 and to periods of reduced rainfall as indicated by low SPI values (gray bars in Fig. 9).

8. The PGH-1 paleoclimatic record

Multi-proxy data from the PGH-1 stalagmite provide evidence of environmental changes in northern India over the past ca 750 years. Deposition of aragonite from AD 1256 to 1489 and after AD 1889 suggests drier conditions and/or more evaporation due to higher temperatures. Dominant calcite, lesser bands of aragonite, and lateral transition from calcite to aragonite along layers in the period AD 1489–1889 indicate a generally cold and slightly wetter early LIA from AD 1489–1730 followed by cold but drier conditions from AD 1730–1889. Higher concentrations of P and S/Sr during periods of aragonite deposition is powerful evidence of more rapid outgassing of CO_2 and increased evaporation leading to rapid supersaturation of precipitating waters and therefore rapid carbonate precipitation. High rates of carbonate precipitation in the aragonite zones may be responsible partly for the higher growth rates in these zones (upper = 0.28 mm/yr; lower = 0.21 mm/yr) than in the calcite-rich zone (0.16 mm/yr), though estimated growth rates do not take into account increased porosity of the aragonite deposits.

Variations in stable isotopes along the central growth axis of the stalagmite further reveal decadal climate variability near Panigarh. In the upper and lower zones of aragonite, isotopic values suggest much drier conditions at AD 1350–1370, 1410–1440 and 1889–1945. The first two periods of dryness are recorded in dense aragonite while the third is in mixed porous and dense aragonite (Fig. 6E). Lower $\delta^{18}O$ values indicate wetter conditions at AD 1250–1350, 1370–1410, and even more precipitation at AD 1450–1480 and 1945–1995, the last period followed by slightly drier conditions until 2005. In fact there is a gradual decrease in $\delta^{18}O$ values from AD 1800 to 1970 that records an increase in precipitation amount possibly related to stronger ISMs. The lowest $\delta^{18}O$ values in the entire record are centered at AD 1970 suggesting that this interval was the wettest of the past ~750 years. However around AD 1920 there was a short interval of much drier conditions possibly indicating a weaker monsoon. After AD 1970 a steady

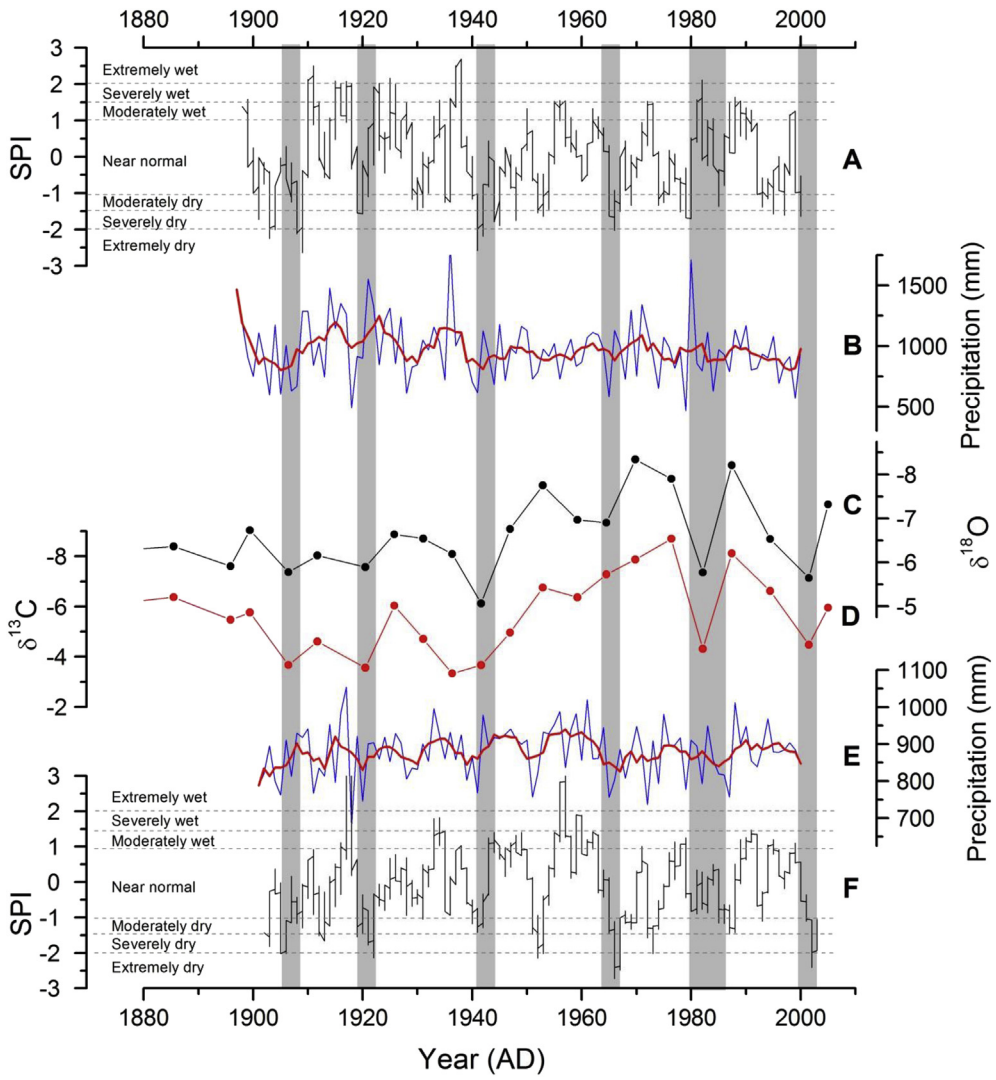

Fig. 9. Trends in PGH-1 carbonate $\delta^{18}O$ (C) and $\delta^{13}C$ (D) values compared with annual Mukteshwar (B) and all India (E) (thin blue lines) and 5-year mean (thicker red lines) monsoon precipitation, and the 24-month-SPI of Mukteshwar (A) and all India (F) monthly precipitation from ~1901 to 2000. The SPI values were calculated using the method of McKee et al. (1993) for all India (Guhathakurta and Rajeevan, 2008) and Mukteshwar (Kotlia et al., 2012) monthly precipitation data. Dry and wet rainfall intensities (near normal, moderately dry/wet, severally dry/wet, and extremely dry/wet) were defined using the SPI values following the classification scheme proposed by McKee et al. (1993). Shaded areas show examples where low rainfall/SPI values and high isotope values coincide. In general higher isotope values are associated with decreased precipitation and lower values with reduced precipitation. (For interpretation of the references to color in this figure legend, the reader is referred to the web version of this article.)

increase in stalagmite $\delta^{18}O$ values may record drier conditions. Even within relatively dry periods detrital layers indicate that sometimes, such as at AD 1900, there was a rapid flow of water into the cave. The AD 1900 event left its mark on PGH-1 in the form of aragonite with low luminescence, darker color, and lower $\delta^{18}O$ (Fig. 6E).

Within the central, calcite-rich section of PGH-1, which corresponds approximately with the LIA, higher $\delta^{18}O$ values indicate dry intervals at AD 1630–1675, 1725–1755, and 1810–1889. However, this last dry interval may not have been as dry as the period immediately following in the upper aragonite zone at 1889–1945. The wettest period in the central calcite zone is in dense calcite and lasted from about AD 1490–1630. The driest period is in the upper section of the calcite-rich zone characterized by calcite on the growth axis and aragonite on the flanks of the stalagmite. This period corresponds with generally higher $\delta^{18}O$ values also indicative of drier conditions, despite the presumed colder temperatures that caused calcite rather than aragonite deposition. Separating these upper and lower calcite zones is detritus-rich calcite with generally lower $\delta^{18}O$ values indicating more moisture.

In general low $\delta^{18}O$ values, which we interpret as indicating wetter conditions, are accompanied by low luminescence and low reflectance in all fabrics of both calcite and aragonite. We believe this is because darker colors record an increase in detrital material and higher density of deposit resulting in low luminescence also. Low $\delta^{18}O$ values are also accompanied by low $\delta^{13}C$ values because of higher soil CO_2 in wetter conditions and less carbon with high $\delta^{13}C$ coming from the carbonate bedrock. In contrast, high $\delta^{18}O$ and $\delta^{13}C$ indicate drier conditions with low levels of soil CO_2 and thus more carbon coming from the bedrock.

If calcite was deposited on PGH-1 during cooler conditions at the time of the LIA, then the LIA lasted in the northern India Himalayan foothills from AD 1490–1890. However, if we define the LIA boundaries where there are marked shifts in stalagmite $\delta^{18}O$ and $\delta^{13}C$ values, representing rapid changes in climate, the LIA lasted from about AD 1450–1820, and the MCA, which preceded the LIA, began before AD 1256 and ended around AD 1450.

An important conclusion from the PGH-1 data is that near

Panigarh cave the early LIA, from about AD 1450–1650, was wetter than the later LIA, which was drier as indicated by a transition to aragonite deposition on the flanks of the stalagmite with calcite at the growth axis. In contrast, the MCA and the post-LIA period were drier than the LIA, as indicated by aragonite, rather than calcite deposition, and by higher $\delta^{18}O$ and $\delta^{13}C$ values. However, although the LIA was wetter than the preceding and following periods, conditions fluctuated between wetter and drier at decadal intervals, as evidenced by frequent aragonite layers within the calcite zone.

9. Regional paleoclimatic patterns: PGH-1 and other proxy climate records

9.1. Stalagmites

Cave stalagmite evidence from India and China (Fig. 1) suggests that after ~AD 1250 opposite conditions prevailed in northern areas compared to southern areas influenced by the Asian Monsoon (Fig. 6); when the north was wetter (drier) the south was drier (wetter).

The records for the ISM core area (Sinha et al., 2007, 2011), and the EAM core area (Wang et al., 2005) suggest somewhat wetter conditions (lower $\delta^{18}O$ values) prior to ~AD 1500, during what may be the MCA in this area, followed by drier conditions (higher $\delta^{18}O$ values) from ~AD 1500 to 1700, and then by higher precipitation to the present (Fig. 6G). In contrast, the PGH-1 and WahShikar (located close to the northern margin of ISM), and Dayu cave (northern boundary of the EAM) records have higher $\delta^{18}O$ values (drier conditions) prior to AD 1460/1520 during the MCA, followed by lower $\delta^{18}O$ values (wetter conditions) from AD 1460/1510 to ~AD 1660 when values increase rapidly over the next ~100 years and then remain relatively high until ~AD 1920 (Fig. 6D). The PGH-1 record parallels the WahShikar cave record (Sinha et al., 2011) as does stalagmite isotope data from Chularasim Cave (Kotlia et al., 2012), all showing a shift towards higher $\delta^{18}O$ values, and thus drier conditions in the foothills of the Himalayas in the late 1600s, following a period of wetter conditions during the early part of the LIA.

The shift towards drier conditions in northern India in the late 1600s is recorded in stalagmite PGH-1 by a change from dense calcite to detritus-rich calcite and later to calcite on the growth axis and aragonite on the flanks of the stalagmite. At both Panigarh and WahShikar cave, this trend is interrupted temporarily by a short interval of increased wetness from ~AD 1680–1720. Most likely, the detritus-rich calcite is a response to increasingly dry conditions above Panigarh cave, leading to a reduced cover of vegetation that facilitated erosion of detrital material after rain. The increased aridity eventually led to aragonite forming on the flanks of PGH-1 with calcite at the crest.

Stalagmites from Siddha Baba cave in the Pokhara Valley, central Nepal (27°59′N; 84°49′E), have dense, optically clear calcite layers from AD 1550–1640 that indicate a less-evaporative cave environment than previously and moister and/or cooler conditions (Denniston et al., 2000). This change essentially parallels the change from aragonite to calcite in the PGH-1 stalagmite at ~AD 1450, at the beginning of the LIA that appears to have been accompanied by a shift to a wetter climate in the foothills of the Himalayas.

Cave records in China, also appear to record a dry early LIA in the south and at the same time wet conditions further north, with the Dongge and Dayu isotope records being examples of this difference (Figs. 1 and 6). Additional evidence of early LIA wet conditions in the north comes from Shihua cave in northeast China (Ku and Li, 1998) and Buddha cave in north central China (Paulsen et al., 2003). Lower $\delta^{18}O$ values in a stalagmite from Dayu cave, in the south flank of the Qinling Mountains, indicate higher precipitation from AD 1535 to 1685 (Tan et al., 2009). In contrast, to the south, a drier early LIA is documented in stalagmites from Akalagavi cave (Yadava et al., 2004), Dandak and Jhumar caves (Sinha et al., 2007, 2011) from Peninsular India and Wanxiang (Zhang et al., 2008), Heshang (Hu et al., 2008), and Dongge cave (Wang et al., 2005) from China (Fig. 1).

9.2. Other paleoenvironmental proxies

The spatial pattern of precipitation suggested by the stalagmite data (see also Sinha and Berkelhammer, 2010), with northern areas receiving higher (lower) precipitation when southern areas receive lower (higher) precipitation is also apparent in non-stalagmite proxy climate records.

For example, a pollen study in the Pinder Valley near Panigarh cave shows a change towards moist conditions from ~AD 1540 to 1799 (Rühland et al., 2006), coincident with calcite deposition on the PGH-1 stalagmite. Cooler conditions during the LIA are indicated by tree ring records for the western Himalayas for the period AD 1600–1950 (Yadav and Singh, 2002) and for Nepal from AD 1605 to 1770 (Cook et al., 2003). Clearly, the evidence of a cold and wet LIA in the Himalayas correlates well with deposition of calcite on stalagmites in Panigarh cave in northern India and Siddha Baba cave in central Nepal (Denniston et al., 2000) during this time interval, with colder temperatures and increased moisture favoring the deposition of calcite over aragonite. In central and south India the evidence is largely of a drier LIA except in the extreme south where even a weak monsoon still brings good rains. By contrast, Kale and Baker (2006) note an absence of high-magnitude slack water flood deposits in six large rivers in central and western India and they argue that the period from the 14th to 19th centuries was probably drier.

Records from the Qinghai–Tibet Plateau also show a wetter LIA. For example, variations in snow accumulation on the Guliya Ice Cap indicate a moist climate from AD 1500 to 1880 (Yao et al., 1996), while high pollen concentrations and relatively low *Artemisia*/*Chenopodiaceae* ratios in the Dunde Ice Cap indicate more humid conditions from AD 1400 to present (Liu et al., 1998). A significant increase in decadally averaged snow accumulation in the Dasuopu Ice Cap from AD 1817 to 1880 shows high precipitation and moist conditions during the later part of the LIA (Thompson et al., 2000), with generally lower snow accumulation from AD 1600 to 1817 and after AD 1880. Reduced salinity in Lake Chencuo, southern Tibet, indicated by diatoms, shows that the last cold episode of the LIA, from AD ~1845–1885, was somewhat wetter (Yang et al., 2004). Further north and east, lower concentrations of carbonate and coarser particle sizes in Lake Bosten in Xinjiang Province also suggest that the northern Tibet Plateau was humid from AD 1500 to 1880 (Chen et al., 2006). Higher organic matter and more negative $\delta^{18}O$ values of $CaCO_3$ in Qinghai Lake sediments indicate wetter conditions from AD 1500 to 1950 punctuated by drier episodes from AD 1560 to 1650 and 1780 to 1860 (Zhang et al., 2003). Lower $CaCO_3$concentrations in sediments from Lake Daihai in Inner Mongolia indicate a cold and moist climate during the LIA in north China (Jin et al., 2001). Increased pine pollen and less oak and broad-leaved deciduous tree pollen in a core from the Yangtze prodelta in east China, show that the period AD 1085–1815 was cool and wet (Yi et al., 2006). Variations in 21 major and minor elements in a sediment core from Lake Erhai in Yunnan Province further to the southwest, suggest warmer and drier conditions from AD 1340–1550 and 1890–1950, but cooler and wetter conditions during the LIA from AD 1550–1890 (Chen et al., 2005).

10. Discussion

The stalagmite and other proxy data at sites shown in Fig. 1 show a broad spatial pattern in precipitation over South and East Asia during the LIA with northern areas showing generally increased precipitation and southern areas reduced precipitation. During the MCA, and after the LIA, the stalagmite data suggest this pattern was reversed.

That this pattern of precipitation has occurred frequently in the past is clear from gridded spatial data on droughts in the Monsoon Asia Drought Atlas (MADA). The MADA uses the Palmer Drought Severity Index (PDSI) calculated from tree-ring indices, as an estimate of drought severity for each year of the last millennium. A particularly clear example of the north-to-south patterning of precipitation was during the Strange Parallels Drought of AD 1756–1768, during the LIA, when much of southern India was under severe drought conditions (negative PDSI values) while the Himalayas to the north had positive PDSI values and so was not under drought stress (see Fig. 2B in Cook et al., 2010).

Data from MADA for grid units close to Panigarh and Jhumar cave, namely 78.75° E; 28.75° N and 78.75° E, 21.25° N (Fig. 6A and H), respectively, also confirm the climate changes recorded by PGH-1 and other stalagmites since ~AD 1256. The tree-ring based PDSI time series correlate well with the stalagmite isotope records but what is noticeable is that PDSI variations in the southern grid unit are much more marked than those in the northern grid unit, even when smoothed using a 21-year running mean. This indicates that since ~AD 1256 droughts were never as severe in the north as they were in the south, and wetter periods were never as wet in the north as in the south. What is clear from the MADA data, however, is that major dry intervals, such as those at ~AD 1460, 1680 and 1940, are evident in all of the records depicted in Fig. 6.

However, not all sites over south and east Asia fit the wet in the north and dry in the south LIA model (Fig. 1). Local historical documents and geochemical proxy data from Lake Huguangyan in the Leizhou Penninsula in Guangdong Province also indicate a warmer and drier MCA and a wetter and cooler LIA in tropical coastal south China, while a wetter LIA is indicated by a cave stalagmite in Akalagavi cave in the Western Ghats (Yadava et al., 2004), and a tree-ring record from teak trees in the same area (Borgaonkar et al., 2010). These exceptions to the dry LIA of much of southern India and China show that even a weak monsoon can bring considerable precipitation to coastal sites (Chu et al., 2002). von Rad et al. (1999) document a wetter interval at the time of the LIA in a marine core off Pakistan in the northern Arabian Sea, suggesting that higher rainfall in northern basins of the Indus River catchment, in the Himalayas, was increasing the discharge of the Indus River into the Arabian Sea during the LIA.

Climate shifts in the Indian Central Himalaya as indicated by our PGH-1 records are mainly controlled by variations in ISM intensity. Variations in *Globigerina bulloides* percentages in Arabian Sea core RC 2730 (Anderson et al., 2002), with higher percentages indicating stronger winds and increased upwelling during a more powerful ISM, are correlated with the PGH-1 $\delta^{18}O$ and $\delta^{13}C$ records, and with Dasuopu glacier $\delta^{18}O$ values (Fig. 6). This means that during the early part of the LIA, when the Arabian Sea *G. bulloides* record indicates a weak ISM, conditions were colder in Tibet, and in general over broad areas, there was more precipitation in north China and the foothills of the Himalayas, all at a time when much of southern India and southern China were subjected to drier conditions because of weak monsoons. The marked shift in climate in the late 1600s, noted by Sinha et al. (2011), is paralleled in the Arabian Sea core by a rapid increase in *G. bulloides* percentages after ~AD 1700, indicating stronger ISMs. Paralleling this change is evidence of reduced precipitation at Panigarh cave, and higher temperatures (higher $\delta^{18}O$ values) at the Dasuopu glacier (Fig. 6). All of this evidence suggests that when the ISM and EAM are weak, northern areas of India and China are wetter/colder and southern areas warmer and drier. Arabian Sea core RC 2730 *G. bulloides* percentages show that since ~AD 1256 the ISM was weakest during the early part of the LIA. It was only a little stronger during the preceding MCA, reached intermediate strength during the second cold phase of the LIA centered ~AD 1800, and was most powerful during the warm period of the LIA at ~AD 1750 and since ~AD 1870. All of these changes in the Arabian Sea core are identifiable in the cave, tree-ring and glacier records in Fig. 6, attesting to the importance of ISM strength in determining regional precipitation amounts and patterns.

10.1. Monsoon breaks

Wetter conditions during the LIA in the Indian Central Himalaya could be explained by more monsoon break events during the LIA when the ISM was weaker. Sinha et al. (2011) argued that the wetter conditions in the foothills of the Himalayas from ~AD 1400–1700 could be attributed to a higher frequency and/or amplitude of monsoon break events, and suggest that the simultaneous shift to opposing precipitation regimes in the Jhumar/Dandak records during the late 1600s was caused by a change to a predominantly "active" state, generating precipitation anomalies of the opposite sign over central and northeast India. Thus a possible higher frequency of break conditions during the LIA implies a weaker ISM that brings drier conditions to the core ISM area, but wetter conditions to northern India.

During 'break' conditions the monsoon trough is located close to the foot of the Himalayas, which leads to a striking decrease in rainfall over most of India but to an increase along the Himalayas and parts of northeast India and in the extreme southeast of Peninsular India (e.g. Ramaswamy, 1962; Rao, 1976). Heavy rains do occur in and near the Himalayas, possibly triggered by eastward moving troughs in the westerlies, but these are more common east of 85°E than they are to the west (Panigarh is at ~80°E).

Ramamurthy (1969) surveyed 'breaks' during July and August, the most common months for them to occur, over an 80-year period, 1888–1967. The breaks usually lasted 3–5 days and in the 80 years there were 12 years with no break, 25 years with 1 break/yr, 22 years with 2 breaks/yr, 9 years with 3 breaks/yr, and 2 years with 4 breaks/yr. Ramaswamy (1973) examined normal 'active monsoon' rainfall during August at stations around India and documents increases of around 20% in rainfall in the area near Panigarh cave during 'breaks' compared to active monsoon conditions. At Mukteshwar, he found 'normal' daily rainfall in August to be 9.9 mm/day, while during 'breaks' it rose to a maximum of around 12 mm/day for a few days. To the east in the WahShikar cave area increases were higher, in places by more than 40%. These data suggest that any increase in rainfall in the foothills of the Himalayas near Panigarh and WahShikar cave during the LIA, resulting from more break events, may not have been sufficient (particularly at Panigarh cave west of 85°E) to explain the evidence of higher precipitation in stalagmites from these caves.

10.2. Winter southern jet depressions

A second possible explanation for increased LIA precipitation at Panigarh cave is that there was an increase in winter precipitation due to the Southern Winter Subtropical Jet funneling depressions along the southern margin of the Tibetan Plateau and then into northeast China (Fig. 1). Singh et al. (2009) have examined this possibility by reconstructing spring (March–July) precipitation for Himachal Pradesh in the western Himalayas (~31° 30′ N; 78° 20′ E)

from AD 1310 using tree rings. In this area, the westerlies contribute around 80% of the precipitation in the March–July season. The tree-ring based precipitation reconstruction (AD 1310–2004) shows strong interdecadal variations superimposed over high year-to-year variations but does not show a clear increase in precipitation during the LIA. In a similar study, Singh et al. (2006) produced tree-ring based time series of March–May precipitation in West Uttar Pradesh in the eastern part of the western Himalayas (~30° 30′ N; 79° 30′ E), very close to Panigarh cave, for the period AD 1560–1997. They found that from AD 1560 to the 1850s dry and wet periods were of almost equal duration, showing that the LIA experienced fluctuating spring precipitation in the western Himalayan region (Singh et al., 2006). This agrees remarkably well with our evidence from PGH-1 that from AD 1490 to 1890 deposition was predominantly calcite but with numerous aragonite layers indicating alternating cool/wet (calcite) and perhaps warmer/drier (aragonite) intervals with the former dominating (Fig. 2).

More convincing evidence of increased 'winter' precipitation in the Himalayas, and a possible answer to why the tree-ring data did not show increased precipitation during the LIA in spring, comes from the Dasuopu glacier on the southern rim of the Tibetan Plateau. Davis et al. (2005) report that from ~1880 to the 1990s, summer monsoon precipitation was a significant component of the annual accumulation on the Dasuopu glacier, but during the latter part of the LIA (~1810–~1880) total net snow accumulation was 30% higher than estimated summer monsoon amounts in northern India. They argue that the excess snow during the latter part of the LIA may have been the result of either higher summer precipitation that was not experienced in the core monsoon region to the south (during breaks?), or by higher accumulation rates during the winter. In fact, Davis et al. (2005) suggest that westerly low-pressure systems linked to the North Atlantic could have pushed farther east along the Himalayas than they do today, bringing extra snowfall to the Dasuopu glacier. Winter precipitation today comprises a small percentage of the annual total, and comes from disturbances that occasionally move eastward from the Hindu Kush-western Himalayan mountain complex. The moisture originates in the high latitudes, and is delivered to the Himalayas by frontal systems rather than by deep convection. Thus the mean condensation level is at a lower elevation in winter, resulting in less fractionation and more enriched $\delta^{18}O$ values in precipitation. This could explain why PGH-1 calcite $\delta^{18}O$ values are only slightly lower than values in the older and younger aragonite layers, which were affected by evaporation after predominantly ISM rainfall.

Davis et al. (2005) used spectral analysis to examine periodicities in the pre-1880 and post-1880 Dasuopu glacier net snow accumulation and summer monsoon precipitation. This revealed that North Atlantic processes influenced early winter precipitation during the LIA, and later were replaced by tropical Pacific influences as the recent warming got underway and the monsoon circulation asserted more control over the annual Dasuopu accumulation. After the LIA ended, the winter snow totals in the central Himalayas dropped abruptly as the ISM strengthened, and summer precipitation became more significant. Precipitation fell on the Dasuopu glacier during the LIA in late fall and early winter, not in spring, which was the focus of the tree-ring studies, because today the majority of the winter storms appear from January to March.

In fact, increased winter precipitation during the LIA in the Indian Central Himalaya may also be a result of a weaker ISM. The more frequent monsoon break conditions may also have allowed more westerly disturbances along the foothills of the Himalaya (see Kotlia et al., 2012, 2014; Sanwal et al., 2013) that were enhanced by mountain orography. The cooler LIA would in all likelihood have increased the extent of snow in Asia during the winter, and may even have led to early snows in the region, both known to reduce the strength of the ISM (e.g. Bamzai and Shukla, 1999; Wu and Qian, 2003; Ye et al., 2005). In addition, the lower temperatures would have pushed the belt of westerly disturbances to the south, which may have played a role in the observed increase in winter precipitation in the foothills of the Himalayas and other uplands along the northern edge of the southerly sub-tropical jet stream. Lower temperatures during the LIA are confirmed by higher $\delta^{18}O$ values in ice from the Dasuopu glacier (28° 23′ N; 85° 43′ E) at the southern edge of the Tibetan Plateau (Fig. 6C).

11. Conclusions

Although the PGH-1 stalagmite was probably not deposited under isotopic equilibrium conditions, variations in petrography and stable isotope values along the central growth axis still provide evidence of changes in the ISM over about the last ~750 years. These variations record that in the Himalayan foothills in Western Uttar Pradesh the LIA lasted from AD 1450/1490–1820/1890. The LIA was slightly wetter than the periods before and after but conditions fluctuated at decadal scales from much wetter to much drier. This contrasts with evidence of drought conditions in the core of the ISM in India during the LIA and also in southern China that is affected by the EAM. Western Utter Pradesh may have been slightly wetter than the core ISM area because of an increased number of ISM 'break events' that brought increased rainfall to the mountains during periods of weak ISM that brought drought conditions to the ISM core area. At the same time, depressions originating in the eastern Mediterranean may have been pushed south during the LIA by colder temperatures and carried along the southern margin of the Tibetan Plateau by the southern winter jet. These depressions may have increased winter/spring precipitation in areas beneath the southern track of the subtropical winter jet stream, including the area of the Dasuopu glacier.

Cooler ocean and continental termperatures push the westerlies and associated low pressure systems further south, so that some are carried by the southern winter jet stream along the southern margin of the Tibetan Plateau bringing more precipitation to the foothills of the Himalayas in northern India. In contrast, a warmer Eurasian landmass during the MCA tended to increase the transport of warm water to the North Atlantic, thus warming the ocean and adjacent landmasses. The result was a strengthened pressure gradient between the Indian Ocean and the Eurasian landmass and therefore a stronger ISM. This caused the westerlies to move north, which reduced winter/spring precipitation along the southern boundary of the Tibetan Plateau.

Acknowledgments

This research was supported by a DDR NSF grant 0623407 to Brook and Liang and by funds provided to Brook by the Franklin College of Arts and Sciences, University of Georgia. Kotlia is grateful to the Alexander von Humboldt Foundation (Linkage Project, No 3-4-FoKoop, 396 DEU/1017420) and Ministry of Earth Sciences (MoES/PO/Geosci/43/2015, New Delhi) for financial support and Kandasamy thanks the National Science Foundation of China (No. 41273083), Shanhai Fund (No. 2013SH012) and Open Fund of Tongji University, China (No. MGK1201) for the financial support.

References

Anderson, D.M., Baulcomb, C.K., Duvivier, A.K., Gupta, A.K., 2010. Indian summer monsoon during the last two millennia. J. Quat. Sci. 25 (6), 911–917.
Anderson, D.M., Overpeck, J.T., Gupta, A.K., 2002. Increase in the Asian southwest monsoon during the past four centuries. Science 297, 596–599.
Bamzai, A.S., Shukla, J., 1999. Relation between Eurasian snow cover, snow depth, and Indian Summer Monsoon: an observational study. J. Clim. 12, 3117–3132.

Barry, R.G., Chorley, R.J., 2003. Atmosphere, Weather, and Climate. Holt, Rinehart and Winston, New York.
Borgaonkar, H.P., Sikder, A.B., Ram, S., Pant, G.B., 2010. El Niño and related monsoon drought signals in 523-year-long ring width records of teak (Tectonagrandis L.F.) trees from south India. Palaeogeogr. Palaeoclimatol. Palaeoecol. 285, 74–84.
Brook, G.A., Ellwood, B.B., Railsback, L.B., Cowart, J.B., 2006. A 164 ka record of environmental change in the American southwest from a Carlsbad Cavern speleothem. Palaeogeogr. Palaeoclimatol. Palaeoecol. 237, 483–507.
Burton, E.A., Walter, L.M., 1987. Relative precipitation rates of aragonite and Mg calcite from seawater: temperature or carbonate ion control? Geology 15, 111–114.
Cabrol, P., Coudray, J., 1982. Climatic fluctuations influence the genesis and diagenesis of carbonate speleothems in southwestern France. Natl. Speleol. Soc. Bull. 44, 112–117.
Chen, F., Huang, X., Zhang, J., Holmes, J.A., Chen, J., 2006. Humid Little Ice Age in arid central Asia documented by Bosten Lake, Xinjiang, China. Sci. China Ser. D Earth Sci. 49, 1280–1290.
Chen, J., Chen, F., Zhang, E., Brooks, S.J., Zhou, A., Zhang, J., 2009. A 1000-year chironomid-based salinity reconstruction from varved sediments of Sugan Lake, Qaidam Basin, arid Northwest China, and its palaeoclimatic significance. Chin. Sci. Bull. 54 (20), 3749–3759.
Chen, J., Wan, G., Zhang, D.D., Chen, Z., Xu, J., Xiao, T., Huang, R., 2005. The 'Little Ice Age' recorded by sediment chemistry in Lake Erhai, southwest China. Holocene 15, 925–931.
Cheng, H., Edwards, R.L., Hoff, J., Gallup, C.D., Richards, D.A., Asmerom, Y., 2000. The half-lives of uranium-234 and thorium-230. Chem. Geol. 169, 17–33.
Chu, G., Liu, J., Sun, Q., Lu, H., Gu, Z., Wang, W., Liu, T., 2002. The 'Mediaeval Warm Period' drought recorded in Lake Huguangyan, tropical South China. Holocene 12, 511–516.
Cook, E.R., Krusic, P.J., Jones, P.D., 2003. Dendroclimatic signals in long tree-ring chronologies from the Himalayas of Nepal, Int. J. Climatol. 23, 707–732.
Cook, E.R., Anchukaitis, K.J., Buckley, B.M., D'Arrigo, R.D., Jacoby, G.C., Wright, W.E., 2010. Asian monsoon failure and mega drought during the last millennium. Science 328, 486–489.
Davis, M.E., Thompson, L.G., Yao, T., Wang, N., 2005. Forcing of the Asian monsoon on the Tibetan Plateau: evidence from high-resolution ice core and tropical coral records. J. Geophys. Res. 110, D04101. http://dx.doi.org/10.1029/2004JD004933.
Denniston, R.F., Gonzalez, L.A., Asmerom, Y., Sharma, R.H., Reagan, M.K., 2000. Speleothem evidence for changes in Indian summer monsoon precipitation over the last ~2300 years. Quat. Res. 53 (2), 196–202.
Duan, W., Kotlia, B.S., Tan, M., 2013. Mineral composition and structure of the stalagmite laminae from Chulerasim cave, Indian Himalaya and the significance for palaeoclimatic reconstruction. Quat. Int. 298, 93–97.
Edwards, R.L., Chen, H., Wasserburg, G.J., 1987. ^{238}U–^{234}U–^{230}Th–^{232}Th systematics and the precise measurement of time over the past 500,000 years. Earth Planet. Sci. Lett. 81, 175–192.
Fairchild, I.J., Baker, A., Borsato, A., Frisia, S., Hinton, R.W., McDermott, F., Tooth, A.F., 2001. Annual to sub-annual resolution of multiple trace-element trends in speleothems. J. Geol. Soc. (Lond.) 158 (5), 831–841.
Friedman, I., O'Neil, J.R., 1977. Compilation of Stable Isotope Fractionation Factors of Geochemical Interest: U.S. Geological Survey. Professional Paper 440-KK, pp. 1–12.
Grossman, E.L., Ku, T.-L., 1986. Oxygen and carbon isotope fractionation in biogenic aragonite: temperature effects. Chem. Geol. 59, 59–74.
Gupta, A.K., Anderson, D.M., Overpeck, J.T., 2003. Abrupt changes in the Asian southwest monsoon during the Holocene and their links to the North Atlantic Ocean. Nature 421, 354–357.
Guhathakurta, P., Rajeevan, M., 2008. Trends in the rainfall pattern over India. Int. J. Climatol. 28 (11), 1453–1469.
Haq, Z., Choudhury, G., 2014. Why Monsoon Is the Life-blood of Indian Economy. Hindustan Times, New Delhi. Retrieved from. http://www.hindustantimes.com/business-news/why-monsoon-is-the-life-blood-of-indian-economy/article1-1193815.aspx.
Hendy, C.H., 1971. The isotopic geochemistry of speleothems, 1.the calculation of the effects of different modes of formation on the isotopic composition of speleothems and their applicability as paleoclimatic indicators. Geochim. Cosmochim. Acta 35, 801–824.
Hu, C., Henderson, G.M., Huang, J., Xie, Sun, Y., Johnson, K.R., 2008. Quantification of Holocene Asian monsoon rainfall from spatially separated cave records. Earth Planet. Sci. Lett. 266, 221–232.
IPCC Fourth Assessment Report: Climate Change, 2007. In: Solomon, S., et al. (Eds.), The Physical Science Basis. Cambridge University Press. Special Report on Emissions.
Jin, Z.D., Wang, S.M., Shen, J., Zhang, E.L., Li, F.C., Ji, J.F., Lu, X.W., 2001. Chemical weathering since the Little Ice Age recorded in lake sediments: a high-resolution proxy of past climate. Earth Surf. Process Landf. 26, 775–782.
Jimenez-Lopez, C., Romanek, C.S., 2004. Precipitation kinetics and carbon isotope partitioning of inorganic siderite at 25°C and 1 atm. Geochim. Cosmochim. Acta 68, 557–571.
Kotlia, B.S., Sharma, C., Bhalla, M.S., G., Rajagopalan, Subrahmanyam, K., Bhattacharyya, A., Valdiya, K.S., 2000. Palaeoclimatic conditions in the late Pleistocene Wadda Lake, eastern Kumaun Himalaya (India), Palaeogeogr., Palaeoclimatol., Palaeoecol. 162, 105–118.
Kotlia, B.S., Ahmad, S.M., Zhao, J.-X., Raza, W., Collerson, K.D., Joshi, L.M., Sanwal, J., 2012. Climatic fluctuations during the LIA and post-LIA in the Kumaun Lesser Himalaya, India: evidence from a 400 y old stalagmite record. Quat. Int. 263, 129–138.
Kotlia, B.S., Singh, A.K., Joshi, L.M., Dhaila, B.S., 2014. Precipitation variability in the Indian Central Himalaya during last ca. 4,000 years inferred from a speleothem record: impact of Indian Summer Monsoon (ISM) and Westerlies. Quat. Int. http://dx.doi.org/10.1016/j.quaint.2014.10.066.
Ku, T., Li, H., 1998. Speleothems as high-resolution paleoenvironment archives: records from northeastern China. Proc. Indian Acad. Sci. (Earth Planet. Sci.) 107 (4), 321–330.
Lambert, W.J., Aharon, P., 2011. Controls on dissolved inorganic carbon and $\delta^{13}C$ in cave waters from DeSoto Caverns: Implications for speleothem $\delta^{13}C$ assessments. Geochim. Cosmochim. Acta 75, 753–768.
Lauritzen, S.-E., Ford, D.C., Schwarz, H.P., 1986. Humic substances in speleothems matrix-paleoclimate significance. In: Proceedings of the 9th International Congress of Speleology, vol. 2, pp. 77–79. Barcelona, August, 1986.
Liu, K.-b., Yao, Z., Thompson, L.G., 1998. A pollen record of Holocene climatic changes from the Dunde ice cap, Qinghai-Tibetan Plateau. Geology 26, 135–138.
Mann, M.E., Cane, M.A., Zebiak, S.E., Clement, A., 2005. Volcanic and solar forcing of the tropical Pacific over the past 1000 years. J. Clim. 18, 447–456.
McKee, T.B., Doesken, N.J., Kleist, J., 1993. The relationship of drought frequency and duration to time scales. In: Proceedings of the 8th Conference on Applied Climatology. American Meteorological Society, Boston, MA, USA, pp. 179–183.
Mills, P.J., 1965. Petrography of Selected Speleothems of Carbonate Caverns. Unpublished M.S. thesis. University of Kansas, p. 47.
Murray, J.W., 1954. The deposition of calcite and aragonite in caves. J. Geol. 62, 481–492.
Parthasarathy, B., Munot, A.A., Kothawale, D.R., 1995. Monthly and Seasonal Rainfall Series for All-India Homogeneous Regions and Meteorological Subdivisions: 1871–1994. Contributions from Indian Institute of Tropical Meteorology, Pune, India. Research Report RR-065.
Paulsen, D.E., Li, H.-C., Ku, T.-L., 2003. Climate variability in central China over the last 1270 years revealed by high-resolution stalagmite records. Quat. Sci. Rev. 22, 691–701.
Railsback, L.B., 1999. Patterns in the compositions, properties, and geochemistry of carbonate minerals. Carbonates Evaporites 14, 1–20.
Railsback, L.B., Brook, G.A., Chen, J., Kalin, R., Fleisher, C.J., 1994. Environmental controls on the petrology of a late Holocene speleothem from Botswana with annual layers of aragonite and calcite. J. Sediment. Res. A64, 147–155.
Railsback, L.B., Liang, F., VidalRomaní, J.R., Grandal-d'Anglade, A., Vaqueiro Rodríguez, M., Santos Fidalgo, L., Fernández Mosquera, D., Cheng, H., Edwards, R.L., 2011. Petrographic and isotopic evidence for Holocene long-term climate change and shorter-term environmental shifts from a stalagmite from the Serra Do Courel of northwestern Spain, and implications for climatic history across Europe and the Mediterranean. Palaeogeogr. Palaeoclimatol. Palaeoecol. 305, 172–184.
Ramamurthy, K., 1969. Some aspects of the break in the Indian southwest monsoon during July and August. In: Forecasting Manual. India Meteorology Department, Pune, India, pp. 1–57. No. IV-18.3.
Ramaswamy, C., 1962. Breaks in the Indian summer monsoon as a phenomenon of interaction between the easterly and the sub-tropical westerly jet streams. Tellus XIV (3), 337–349.
Ramaswamy, C., 1973. A normal period of large-scale break in the southwest monsoon over Indian current. Science 42, 517–523.
Ramseyer, K., Miano, T., D'Orazio, V., Wildberger, A., Wagner, T., Geister, J., 1997. Nature and origin of organic matter in carbonates from speleothems, marine cements and coral skeletons. Org. Geochem. 26, 361–378.
Rao, Y.P., 1976. Southwest Monsoon. Meteorological Monograph Synoptic Meteorology No. 1/1976. India Meteorology Department, Pue, p. 367.
Reams, M.W., 1972. Deposition of Calcite, Aragonite, and clastic sediments in a Missouri cave during four and one-half years. Natl. Speleol. Soc. Bull. 34, 137–141.
Romanek, C.S., Grossman, E.L., Morse, J.W., 1992. Carbon isotopic fractionation in synthetic aragonite and calcite: effects of temperature and precipitation. Geochim. Cosmochim. Acta 56, 419–430.
Rühland, K., Phadtare, N.R., Pant, R.K., Sangode, S.J., Smol, J.P., 2006. Accelerated melting of Himalayan snow and ice triggers pronounced changes in a valley peatland from northern India. Geophys. Res. Lett. 33, L15709. http://dx.doi.org/10.1029/2006GL026704.
Sanwal, J., Kotlia, B.S., Rajendran, C., Ahmad, S.M., Rajendran, K., Sandiford, M., 2013. Climatic variability in central Indian Himalaya during the last 1800 years: evidence from a high resolution speleothem record. Quat. Int. 304, 183–192.
Selvaraj, K., Parthiban, G., Chen, C.T.A., Lou, J.Y., 2010. Anthropogenic effects on sediment quality off southwestern Taiwan: assessing the sediment core geochemical record. Cont. Shelf Res. 30, 1200–1210.
Shen, C.-C., Edwards, R.L., Cheng, H., Dorale, J.A., Thomas, R.B., Moran, S.B., Weinstein, S., Edmonds, H.N., 2002. Uranium and thorium isotopic and concentration measurements by magnetic sector inductively coupled plasma mass spectrometry. Chem. Geol. 185, 165–178.
Shopov, Y.Y., Ford, D.C., Schwarcz, H.P., 1994. Luminescent microbanding in speleothems: high-resolution chronology and paleoclimate. Geology 22, 407–410.
Siegel, F.R., 1965. Aspects of calcium carbonate deposition in Great Onyx Cave, Kentucky. Sedimentology 4, 285–299.
Siegel, F.R., Dort Jr., W., 1966. Calcite-aragonite speleothems from a hand-dug cave

in northeast Kansas. Int. J. Speleol. 2, 165–169.
Singh, J., Park, W.-K., Yadav, R.R., 2006. Tree-ring-based hydrological records for western Himalaya, India, since A.D. 1560. Clim. Dyn. 26, 295–303.
Singh, J., Yadav, R.R., Wilmking, M., 2009. A 694-year tree-ring based rainfall reconstruction from Himachal Pradesh, India. Clim. Dyn. 33, 1149–1158.
Sinha, A., Berkelhammer, M., 2010. Emerging proxy evidence for coherent failures of the summer monsoons of Asia during the last millennium. PAGES News 18 (2), 85–87.
Sinha, A., Berkelhammer, M., Stott, L., Mudelsee, M., Cheng, H., Biswas, J., 2011. The leading mode of Indian Summer Monsoon precipitation variability during the last millennium. Geophys. Res. Lett. 38, 15703. http://dx.doi.org/10.1029/2011GL047713.
Sinha, A., Cannariato, K.G., Stott, L.D., Cheng, H., Edwards, R.L., Yadava, M.G., Ramesh, R., Singh, I.B., 2007. A 900-year (600 to 1500 AD) record of the Indian summer monsoon precipitation from the core monsoon zone of India. Geophys. Res. Lett. 34, 16707. http://dx.doi.org/10.1029/2007GL030431.
Tan, L., Cai, Y., Cheng, H., An, Z., Edwards, R.L., 2009. Summer monsoon precipitation variations in central China over the past 750 years derived from a high-resolution absolute-dated stalagmite. Paleaogeogr. Palaeoclimatol. Palaeoecol. 280, 432–439.
Thompson, L.G., Yao, T., Mosley-Thompson, E., Davis, M.E., Henderson, K.A., Lin, P.N., 2000. A high-resolution millennial record of the South Asian Monsoon from Himalayan ice cores. Science 289, 1916–1919.
Thrailkill, J., 1971. Carbonate deposition in Carlsbad Caverns. J. Geol. 79, 683–695.
vanBeynen, P., Bourbonniere, R., Ford, D.C., Schwarcz, H.P., 2001. Causes of colour and fluorescence in speleothems. Chem. Geol. 175, 319–341.
Kale, V.S., Baker, V.R., 2006. An extraordinary period of low-magnitude floods coinciding with the Little Ice Age: Palaeoflood evidence from central and western India. J. Geol. Soc. India 68 (3), 477–483.
von Rad, U., Schaaf, M., Michels, K.H., Schulz, H., Berger, W.H., Sirocko, F., 1999. A 5000-yr record of climate change in varved sediments from the oxygen minimum zone off Pakistan, Northeastern Arabian Sea. Quat. Res. 51, 39–53.
Vuille, M., Werner, M., Bradley, R.S., Keimig, F., 2005. Stable isotopes in precipitation in the Asian monsoon region. J. Geophys. Res. 110, D23108. http://dx.doi.org/10.1029/2005JD006022.
Wang, Y., Cheng, H., Edwards, R.L., He, Y., Kong, X., An, Z., Wu, J., Kelly, M.J., Dykoski, C.A., Li, X., 2005. The Holocene Asian Monsoon: links to solar changes and North Atlantic climate. Science 308, 854–857.
Webster, J.W., Brook, G.A., Railsback, L.B., Cheng, H., Edwards, R.L., Alexander, C., Reeder, P.P., 2007. Stalagmite evidence from belize indicating significant droughts at the time of preclassic abandonment, the Maya hiatus, and the classic Maya Collapse. Palaeogeogr. Palaeoclimatol. Palaeoecol. 250, 1–17.
Wu, T.-W., Qian, Z.-A., 2003. The relation between the Tibetan winter snow and the Asian Summer Monsoon and rainfall: an observational investigation. J. Clim. 16, 2038–2051.
Yadav, R.R., Singh, J., 2002. Tree-ring-based spring temperature patterns over the past four centuries in western Himalaya. Quat. Res. 57, 299–305.
Yadava, M.G., Ramesh, R., 2005. Monsoon reconstruction from radiocarbon dated tropical Indian speleothems. Holocene 15, 48–59.
Yadava, M.G., Ramesh, R., Pant, G.B., 2004. Past monsoon variations in peninsular India recorded in a 331-year-old speleothem. Holocene 14 (4), 517–524.
Yang, X.D., Wang, S.M., Kamenik, C., Schmidt, R., Shen, J., Zhu, L.P., Li, S.F., 2004. Diatom assemblages and quantitative reconstruction for paleosalinity from a sediment core of Chencuo Lake, southern Tibet. Sci. China Ser. D (Earth Sci.) 47 (6), 522–528.
Yao, T., Thompson, L.G., Qin, D., Tian, L., Jiao, K., Yang, Z., Xie, C., 1996. Variations in temperature and precipitation in the past 2000 a on the Xizang(Tibet) Plateau-Guliya ice core record. Sci. China Ser. D (Earth Sci.) 39, 425–433.
Ye, H., Bao, Z., Feng, X., 2005. Connections of Siberian snow onset dates to the following summer's monsoon conditions over Southeast Asia. Int. J. Climatol. 25, 1567–1584.
Yi, S., Saito, Y., Chen, Z., Yang, D.Y., 2006. Palynological study on vegetation and climatic change in the subaqueous Changjiang (Yangtze River) delta, China, during the past about 1600 years. Geosci. J. 10 (1), 17–22.
Yonge, C.J., Ford, D.C., Gray, J.P., Schwarcz, H.P., 1985. Stable isotope studies of cave seepage water. Chem. Geol. (Isotope Geosci. Sect.) 58, 97–105.
Zhang, J.W., Jin, M., Chen, F.H., Battarbee, R.W., Henderson, A.C.G., 2003. High-resolution precipitation variations in the Northeast Tibetan Plateau over the last 800 years documented by sediment cores of Qinghai Lake. Chin. Sci. Bull. 48, 1451–1456.
Zhang, P., Cheng, H., Edwards, R.L., Chen, F., Wang, Y., Yang, X., Liu, J., Tan, M., Wang, X., Liu, J., An, C., Dai, Z., Zhou, J., Zhang, D., Jia, J., Jin, L., Johnson, K.R., 2008. A test of climate, sun, and culture relationships from an 1810-year Chinese cave record. Science 322, 940–942.